WestVirginiaUniversity
THE RESEARCH REPOSITORY @ WVU

Graduate Theses, Dissertations, and Problem Reports

2021

Design of a Heat Exchanger for a Supercritical CO2 Turbine System

Kehinde Oluwatobi Adenuga
West Virginia University, koa0003@mix.wvu.edu

Follow this and additional works at: https://researchrepository.wvu.edu/etd

 Part of the Heat Transfer, Combustion Commons

Recommended Citation

Adenuga, Kehinde Oluwatobi, "Design of a Heat Exchanger for a Supercritical CO2 Turbine System" (2021). *Graduate Theses, Dissertations, and Problem Reports*. 8151.
https://researchrepository.wvu.edu/etd/8151

This Thesis is protected by copyright and/or related rights. It has been brought to you by the The Research Repository @ WVU with permission from the rights-holder(s). You are free to use this Thesis in any way that is permitted by the copyright and related rights legislation that applies to your use. For other uses you must obtain permission from the rights-holder(s) directly, unless additional rights are indicated by a Creative Commons license in the record and/ or on the work itself. This Thesis has been accepted for inclusion in WVU Graduate Theses, Dissertations, and Problem Reports collection by an authorized administrator of The Research Repository @ WVU. For more information, please contact researchrepository@mail.wvu.edu.

Design of a Heat Exchanger for a Supercritical CO_2 Turbine System

Kehinde Adenuga

Thesis submitted to the Benjamin M. Statler College of Engineering and Mineral Resources at West Virginia University

In partial fulfillment of the requirements for the degree of Master of Science in Mechanical Engineering

Hailin Li, Ph.D., Chair.

Kenneth H Means, Ph.D

Songgang Qiu, Ph.D

Department of Mechanical and Aerospace Engineering

Morgantown, West Virginia

2021

Keywords: Supercritical CO_2, Heat exchanger, Pressure drop, Heat transfer coefficient, Thermal analysis

Copyright 2021 Kehinde Adenuga

ABSTRACT

Design of a Heat Exchanger for a Supercritical CO_2 Turbine System

Kehinde Adenuga

This research aims at designing a shell and tube heat exchanger which will drive a turbine operated on supercritical CO_2. Hot gases from boiler (simulated using air) at 1500 K is introduced into the shell to heat up the supercritical CO_2 at 10 MPa flowing within tubes from 450 K to 1050 K. The design was done using selected shell and tube heat exchanger empirical equations at predefined boundary conditions. The effect of shell and tube diameter on other design parameters was examined. It was observed that the number of tubes, tube external and internal side surface area, volumes of shell and tube, overall surface area and mass of tube material increases as the shell diameter increases from 6 m to 18 m at 2 m interval and this is due to the increase in cross sectional area. The shell length, the number of baffles, overall heat transfer coefficient, the pressure drop in both shell and tube sides all decreases as shell diameter increases at same rate as described previously, and this is attributed to a reduced velocity caused by the increased cross section area of tubes and baffle space. The increase in tube diameter from 0.0092 m to 0.12 m at 0.02 m intervals however leads to an increase in shell length, volume of tube material, number of baffles, shell side pressure drop, tube side pressure drop, overall area of the device ,tube external side surface area and tube internal side surface area. However, the overall heat transfer coefficient, total length of tubes and number of tubes decreases as the tube diameter increases at same rate as described previously. A decision was made on the selected heat exchanger based on fewer tubes, reduced mass of tube materials , low shell and tube pressure drop, and a high heat transfer coefficient. A selected geometry of shell diameter 8 m, shell length 51.62 m, tube diameter 0.102 m, number of tubes 1509 and overall heat transfer coefficient 60.51 W/m^2K was considered.

A CFD analysis was conducted using ANSYS 18.1 on the prototype of the selected heat exchanger device. The device geometry was built using the design modeler and it consist of the shell, tubes, air fluid, CO_2 fluid and baffles The meshing and naming of unit parts was done while the set-up stage was achieved with the predefined boundary conditions and properties. The temperature distribution and thermal analysis of the heat exchanger was reported.

ACKNOWLEDGEMENTS

First and foremost, all glory to God who has given me the grace and strength to start and finish this work. I would like to appreciate my parents Mr. and Mrs. M.M. Adenuga who has put so much efforts and resources in aiding me through my tertiary education journey. I would like to appreciate my advisor Dr. Hailin Li for his persistent efforts towards the success of this thesis. Appreciation to my committee member Dr. Songgang Qiu and Dr. Kenneth H Means for their support, help and input towards this thesis, and for the knowledge transferred. My regards also to Dr. Sam Mukdadi for allowing me work as a teaching assistance under his supervision. I also want to thank Dr. Slava Akkerman and Dr Adam Alas for their effective teachings and contributions regarding my course work.

My regards also to my colleagues Gideon Udochukwu, Samuel Ogunfuye and Lateef Kareem for their input and contribution during the process of writing this thesis work. I appreciate you all and am grateful. Finally, my appreciation goes to Pastor and Mrs. Adeniyi Adebisi and the RCCG Morgantown family for their support in the course of my graduate education at West Virginia University.

Table of Contents

LIST OF FIGURES

LIST OF TABLES

LIST OF VARIABLES

A_c=Shaded area

A_i=Tube internal side surface area

A_o=Tube external side surface area

$A_{overall}$=Overall heat transfer surface area

A_s=Crossflow area of shell

AUR=Air utilization ratio

B=Baffle space

c=Corrosion allowance

CL=Tube layout constant

c_p=Specific heat capacity

CTP=Tube count constant

D_e=Equivalent diameter

d_o=Outer tube diameter

d_i=Inner tube diameter

D_s=Shell diameter

f=Friction factor

f_c=Material allowable stress of the material of construction

F_d=Design factor

F_e=Longitudinal joint factor

F_t=Temperature derating factor

h_i=Heat transfer coefficient of CO_2

h_o =Heat transfer coefficient of air

J=Joint efficiency

k=Thermal conductivity

k_{inc}=Inconel conductivity

L=Length of shell

$\dot{m}$=Mass flow rate

Nu=Nusselt number

N_t=Tube number

N_p= Number of passes

p=Design pressure

PR=Pitch ratio

Pr=Prandtl number

Pt=Tube pitch

Q=Total heat transfer rate

Re_D=Reynold number

S_y=Yield strength of Inconel 617

T_{in}= Inlet temperature

T_{out} = Outlet temperature

ΔT=Temperature difference

t_t=Tube thickness

t_s= Shell thickness

U=Overall heat transfer coefficient

LIST OF GREEK SYMBOLS

Δp_s=Shell side pressure drop

Δp_f =Tube side pressure drop

ΔT_{lm} =Logarithmic mean temperature

ρ =Density

μ =Dynamic viscosity

NOMENCLATURE

ASME: American Society of Mechanical Engineers

CCGT: Combined cycle gas turbine

GE-GR: General Electric Global Research team

GTI: Gas Technology Institute

ORC: Organic Rankine cycle

S-CO_2: Supercritical CO_2

SWRI: Southwest Research Institute

STHXs: Shell tube heat exchangers

1 INTRODUCTION

1.1 Super critical CO_2 power cycle

There are power plants that uses CO_2 in its supercritical state as its working fluid[1]. The supercritical CO_2 (S-CO_2) power cycles have numerous benefits over other working fluid used for thermal and power generating cycles. Firstly, it doesn't go through a constant-temperature boiling process at elevated temperature. Secondly, it has a continuous reduction in density which occurs as the fluid is heated and is abundantly available at a very cheap cost[2]. Also, it is stable in all region of interest and could be set up in a compact style of arrangement. S-CO_2 turbines are very compact and very efficient with small, single casing body design.

Several power cycles are used for power generation and they include Organic Rankine Cycle (ORC), steam Rankine cycle, air Brayton cycle, Combined cycle gas turbine (CCGT), and S-CO_2 direct and indirect cycles[3]. The S-CO_2 based Brayton cycle is a good alternative to the conventional steam power cycles because of high cycle efficiency, compact turbo machinery and compact heat exchangers[4]. A closed Brayton cycle consists five components including a compressor, recuperator, heat exchanger, turbine and precooler. Fluid from the compressor enters recuperator and then to the heat exchanger where the energy from a heat source is transferred into the fluid to drive the shaft in rotary motion[5]. Bryton cycles offers better fuel-power conversion efficiency but requires high turbine inlet temperatures for efficient operation. In [6], at high density of S-CO_2 near the critical point, S-CO_2 Bryton cycles tend to have reduced compressor power consumption and increased efficiency. The S-CO_2 Bryton cycle allows several heat exchangers which include shell and tube, hybrid exchangers, spiral wound exchangers, finned tube and shell exchangers, plate and shell exchangers and porous media exchangers in its operation[7].

The ORC principle is based on a turbo-generator working as a conventional steam turbine to convert the thermal energy into mechanical energy and finally into electric energy through an electrical generator. Instead of generating steam from water, the organic Rankine cycle system vaporizes an organic fluid, characterized by a molecular mass higher than that of water, which leads to a slower rotation of the turbine, lower pressures and no erosion of the metal parts and blades. [8] The ORC uses an organic, high molecular mass fluid with a liquid-vapor phase change , or boiling point, occurring at a lower temperature than the water-steam phase change [9]. The heating of CO_2 is done directly using volumetric and tubular receiver. The indirectly fired closed-loop S-CO_2 cycles [1] has the working fluid heated directly by a heat source through a heat exchanger. Another indirectly heated S-CO_2 cycle is the recuperated closed-loop Brayton cycle. It has a thermal recuperator that is introduced between the turbine and the compressor which helps to improve the cycle efficiency by reducing the heat loss in CO_2 cooler. A semi-closed direct oxyfuel Brayton cycle has the heat exchanger replaced by a pressurized oxy-fuel combustor which burns fuel in oxygen producing CO_2 which is used to drive the turbine [1]. A S-CO_2 power cycle using a shell and tube heat exchanger is shown in Figure 1.1. Hot air simulating hot combustion gases from a boiler move into a shell and tube heat exchanger where thermal energy is transferred to S-CO_2 needed to drive a power generating turbine which produce electricity through a generator.

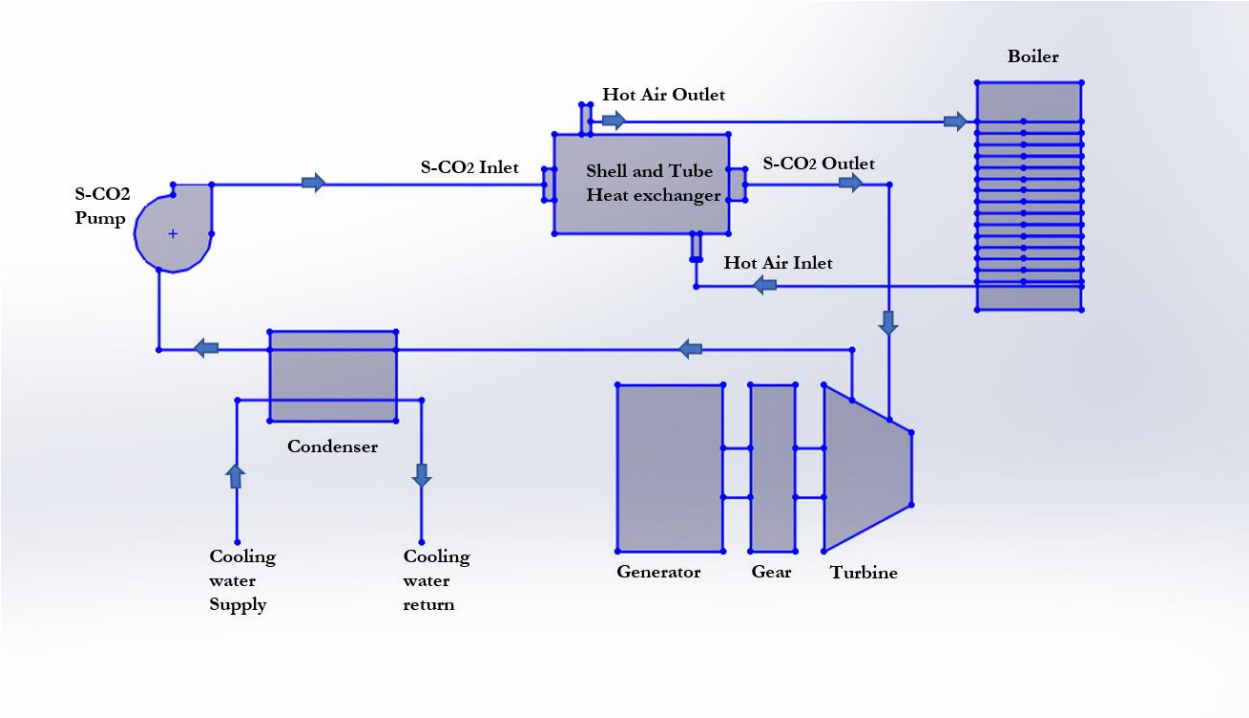

Figure 1. 1: Supercritical CO_2 power cycle

1.2 Objective of this study

The objective of this work is to design a S-CO_2 heat exchanger device. The focus of the study will be at specifying the

i. Design of the heat exchanger in accordance with standard working principles.

ii. Key cost factor and operation parameters such as volume of tube material and pressure drop;

iii. Temperature distribution of the fluids within the shell and tube using CFD.

iv. Temperature distribution within the heat exchanger using CFD.

v. Thermal analysis of the heat exchanger using CFD.

2 LITERATURE REVIEW

Studies on the use of S-CO_2 for power generation have taken place since the 1960s but little or no development was done due to technological limitations [10]. Several publications on heat exchanger design has since surfaced and among which was the design of a tubular type heat exchanger which endures high-temperature and high-pressure conditions under S-CO_2 fluid flow. The device was evaluated using an in-house code, a 3-dimensional flow and thermal stress analysis which aimed at testing the tube integrity. The result indicated that the stress level of the heat exchanger device satisfied the American Society of Mechanical Engineers (ASME) criteria. Further research on S-CO_2 in efficient power generation was conducted in [11]where S-CO_2 direct cycles was compared with conventional Rankine cycles at inlet turbine temperature of 550 °C and 700 °C. A result showing 45 % and 53% efficiency with greater cost reduction was achieved. This shows the benefit of the S-CO_2 direct cycle over other power cycles at different turbine inlet temperature. Generally, it was shown that the efficiency of power plants is directly proportional to the enthalpy of the working fluid at the turbine inlet.

In [12] the US Department of Energy through its supercritical transformational electric power program awarded a $3.9 million project to three design company's which are Echogen Power Systems in Ohio, the Gas Technology Institute (GTI) in Illinois and the Southwest Research Institute (SWRI) in Texas to develop initial plans to design a 10 MW S-CO_2 Brayton Cycle test facility. The project was to support future supercritical Brayton Cycle energy conversion systems which would help achieve national climate and energy goals while promoting domestic job creation and providing the country with a clean and cheaper power. Ongoing work has already been done by SWRI in Texas, the GTI and the General Electric Global Research team (GE-GR) [13][14].They are performing a steady state and transient modelling analysis for a 10 MW S-CO_2 pilot plant test facility using Aspen plus, Aspen

Hysys and Numerical propulsion system simulation software's to arrive at comparable results giving increased confidence in the analysis.

In [15], Zhu reviewed the latest development in S-CO_2 power cycles technologies in relation to power generation. Zhu highlighted the unique properties of S-CO_2 which makes it an ideal working fluid. Zhu also described the types of Brayton cycles with emphasis on the open and closed Brayton cycles. The technical difficulties of the S-CO_2 power cycles were discussed with focus on limited operational experience of S-CO_2 power turbines for commercial operations and challenges experienced in turbo machinery design for equipment operating at elevated turbine inlet temperature.

2.1 Heat exchanger

Heat exchanger is a device used to transfer heat energy between two or more fluids, between a solid particulates or surface and a fluid at different temperatures [16]. They are utilized for controlling heat energy and can regulate efficient heat transfer from one fluid to another. The fluids can be single or two phase and, depending on the exchanger type, it may be separated or in direct contact. In [17], heat exchangers are classified based on flow configuration and by equipment type of construction. The categories based on flow configurations are described in Figure 2.1 and are the counter flow, co-current flow, crossflow and cross/counter flow. Heat exchangers classification by equipment type of construction are either recuperators or regenerators. Recuperators are direct transfer type of heat exchanger where the fluids are separated by wall which prevent mixing or leakage of the fluids. Regenerators are indirect transfer types of heat exchangers where fluid interact via intermittent heat exchange with each other through thermal energy storage. Regenerators normally have fluid leakage due to pressure differences and matrix rotation [16],[17]. The heat exchangers usually seen in our environment are the cooling towers, automobile radiators, condensers, evaporators and air preheaters.

Heat exchangers are classified into various categories such as the classification on transfer process (indirect contact type and direct contact type), number of fluids(two or more fluids), surface compactness (gas to liquid or liquid to liquid and phase change), flow arrangement which include the single-pass and multi-pass arrangements. The multi-pass heat exchanger has the extended surface, shell and tube and plate heat exchangers. The classification based on type of construction have the shell and tube, plate, agitated film and batch pan heat exchangers. Another major classification is on energy utilization (steam and vapor recompression). Lastly is the classification based on reboilers which includes the natural and forced circulation.

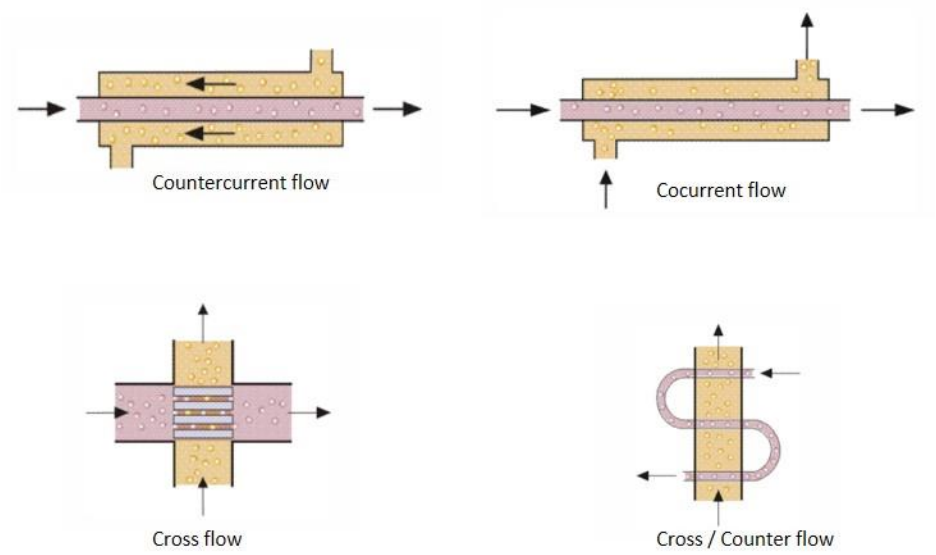

Figure 2. 1: Heat exchanger classification based on flow configuration [17].

2.2 Shell and Tube heat exchanger

Shell and tube heat exchangers (STHXs) are very much in use due to the flexibility they offer for a wide range of temperature and pressure [18]. A shell and tube heat exchanger is made of a large pressure container and several number of tubes inside it. STHXs also have various types of baffles configuration among which are conventional segmental baffles, deflector baffles, disk and doughnut baffles and spaced optimized baffles [19].The design of STHXs include the thermal and mechanical

stage [20], the thermal stage includes the selection of fluids, temperature specification, setting of pressure drops, velocity limits and heat transfer area. The mechanical stage are selection of tube and shell dimensions, setting the tube pitch, tube arrangement, baffle spacing and baffle design.

3 METHODOLOGY

3.1 System description

A shell and tube heat exchanger with straight tubes that are secured at both ends to tubesheets welded to the shell was selected because of its low cost, simple construction and minimal leakage of the shell side fluid. The schematic of the shell and tube heat exchanger is shown in Figure 3.1. The major components are tubes, shell, buffers, flanges, stationary tube sheet, support bracket and shell cover.

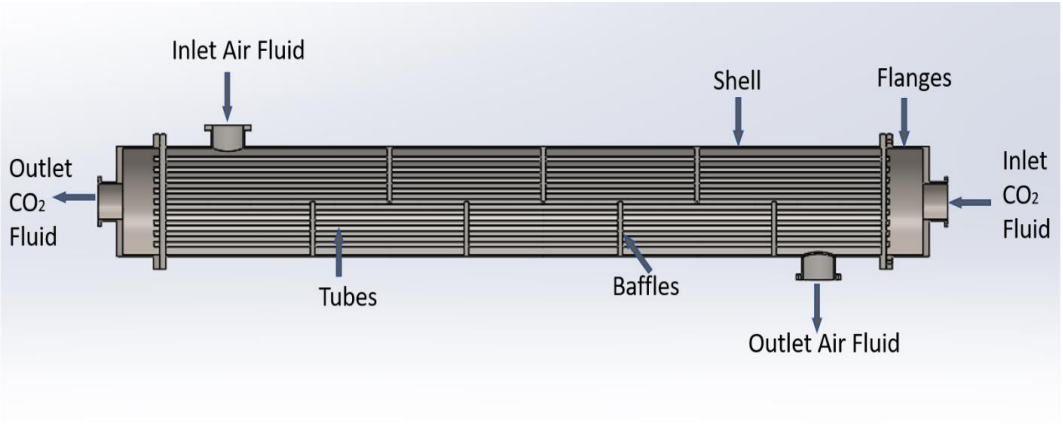

Figure 3.1: Shell and tube heat exchanger

3.1.1 Baffles

Baffles are metal separators used in the shell side of the shell and tube heat exchangers. Baffles are also used to support tubes and enable a desirable velocity for the fluid to be maintained at the shell side and prevent failure of tubes due to flow-induced vibration. Baffles enable better contact of the shell side fluid (air) with the tube surface. They also support the tube bundles and minimize the potential damage caused by flow induced vibration in the tubes.

3.1.2 Baffles spacing

This should have minimum value of one fifth of the shell internal diameter while the maximum baffle spacing should not be greater than the shell internal diameter. Closely placed baffles could mean a

poor penetration of the tubes by shell fluid (air). A large baffle spacing means the shell side fluid (air) flows freely along the direction of the tubes thereby decreasing the heat transfer and overall efficiency. Baffle spacing are normally between 0.3 and 0.6 times of the shell internal diameter. Baffle spaces could also be same size as the shell diameter to achieve a low shell side pressure drop. The baffle spacing for this analysis was set at 0.7 times the shell internal diameter.

3.1.3 Tube layout and pitch

Tubes layout for shell-tube heat exchangers are of two major types, the triangular pattern and the square pattern layouts. The square tube layout shown in Figure 3.3 is used when frequent cleaning is required while the triangular layout is used when more tubes is to be fitted in a given space. Tube pitch is the minimum center to center distance between two tubes. Tube pitch is normally set as 1.25 or 1.5 times tube outer diameter. Tube spacing which helps in controlling shell side pressure drop is given by tube pitch divided by tube diameter ratio. Tube diameter ratio is defined as the tube outer diameter divided by tube inner diameter.

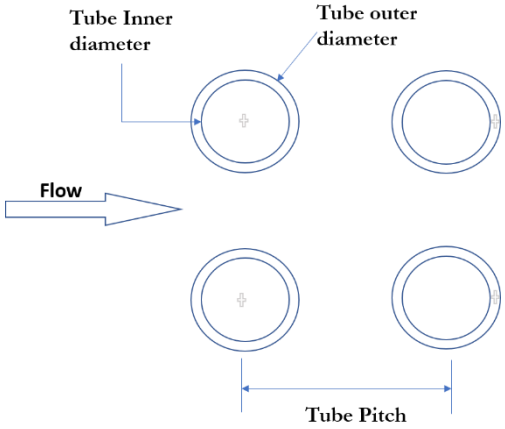

Figure 3.2: Square pitch tube layout

3.1.4 Shell fluid selection

The choice of fluid for the shell side are based on requirement for higher flow rate and higher fluid viscosity which results is needed for increased heat transfer coefficient and overall heat transfer [21].

Air has a high thermal conductivity that increases with temperature [22] and was selected for this design.

3.1.5 Tube material selection

The main factors that influenced the selection of materials for the shell and tube heat exchanger are high thermal conductivity, low coefficient of thermal expansion, high endurance at extreme temperature and pressure conditions, good tensile, good fatigue, corrosion fatigue, creep-fatigue and creep characteristics. The material must have high fatigue toughness and high impact strength to prevent fast cracking [23].The recommended materials for the shell and tube heat exchangers are ferritic steels, austenitic steels, wrought nickel-based steels and the precipitation-strengthened alloy 740 [24]. The nickel-based alloy, Inconel 617 was selected due to its suitability and high endurance at extreme temperature and pressure conditions. It also offers exclusive blend of high strength, oxidation resistance and corrosion resistance at up to 980° C. The physical properties of Nickel based alloys Inconel 617 are listed in Table 3. 1.The chemical composition of Inconel 617 is presented in Table 3.2

Table 3.1: Properties of Inconel 617 at 1000 °C [25]

Inconel 617	Value
Tensile strength	893 MPa
Yield Strength	389 MPa
Tensile Modulus	149 GPa
Shear Modulus	61 GPa
Poisson's ratio	0.3
Specific heat capacity under constant pressure	662 J/kg ·° C
Thermal conductivity	28.7 W/m ·° C
Maximum allowable stress	12.5 MPa
Corrosion resistance	35 g/m^2
Coefficient of expansion	16.3 µm/m·°C
Density	8360 kg/m^3

Table 3.2: chemical composition of Inconel 617, wt. % [25]

Alloy	Ni	Cr	S	B	Ti	Co	Fe	Mn	Mo	Al	Ti	Cu	P	Si	C
Inconel 617	45	22	0.1	0.05	1	13	3	1	9	1.2	0.6	0.5	0.1	1	0.1

3.1.6 Maximum allowable working pressure of the tube

The maximum allowable working pressure of the tube is calculated by equation:

$$P = \frac{2 \times S_y \times F_d \times F_e \times F_t \times \mathrm{t}}{d_i} \quad \text{..... [26]}$$

S_y= yield strength of Inconel 617

F_d=design factor

F_e=longitudinal joint factor

F_t= temperature derating factor

t_t=tube thickness

d_i=inner tube diameter

3.2 Problem description

The model developed in this work solves a steady-state heat transfer problem between a hot flowing air and a counter flow S-CO_2 fluid in a shell and tube heat exchanger configuration. The design is expected to serve a 300 MW gas turbine system with expected thermal efficiency about 50 %. The heat input Q_{in} is projected at 600 MW in order to meet this demand. The $\dot{m}_{CO_2}$ was calculated as 806.74 kg/s using the preset $T_{in,CO_2,}$ and $T_{out,CO_2,}$of 450 K and 1050 K respectively since a moderate

turbine inlet temperature lies between 996 – 1246 K [21]. In order to derive the $\dot{m}_{Air}$, $T_{in,Air}$ was set at 1500 K. A relationship was created between air utilization ratio (AUR), $\dot{m}_{Air}$, $T_{in,Air}$ with the assumption that $T_{out,Air} \geq T_{in,CO_2,}$. After several iterations, a $\dot{m}_{Air}$ of 760 kg/s at $T_{out,Air}$ of 802 K was selected as it offers a suitable geometry design parameter for a effective heat exchanger. Table 3.3 shows the design parameter generated for the shell and tube heat exchanger device.

Table 3. 3: design parameters for the heat exchanger

Design input parameters of the heat exchanger	
CO_2 inlet temperature, (K)	450
CO_2 outlet temperature, (K)	1050
CO_2 mass flow rate (kg/s)	806.74
Air inlet temperature, (K)	1500
Air outlet temperature (K)	802
Air mass flow rate (kg/s)	760.00

The mass flow rate and inlet temperatures were specified at entry positions while the outlet temperatures was specified at exit positions. The alloy Inconel 617 is selected as the material for the shell and tube heat exchanger due to its suitability and high endurance at extreme temperature and pressure conditions [27]. The thermo-physical properties of the fluid domain are constant, and the values of density (ρ) specific heat (c_p)thermal conductivity (k), dynamic viscosity (μ), Prandtl number (Pr) are provided in Table 3.4 and Table 3.5

Table 3. 4: Thermo physical properties of the Air at 1.13 bar [22]

	$T_{h,i}$	$T_{h,o}$	$T_{h,a}$
Temperature (K)	1500	802	1151
ρ , density (kg/m^3)	0.2353	0.6419	0.3209
μ, dynamic viscosity (N. s/m^2)	0.00005264	0.00002849	0.00004511
c_p, specific heat under constant pressure (J/kg. K)	1211.2	1039.8	1167
k, Conductivity (W/m. K)	0.08831	0.04357	0.0733
Pr, Prandtl number	0.722	0.688	0.708

Table 3. 5: Thermo-physical properties of the S-CO_2 at 10 MPa [28]

	$T_{c,i}$	$T_{c,o}$	$T_{c,a}$
Temperature (K)	450	1050	750
ρ, density (kg/m^3)	131.6	49.31	71.5
μ, dynamic viscosity (N. s/m^2)	0.00002358	0.00004285	0.0000315
c_p, specific heat under constant pressure (J/kg. K)	1208.346	1270.7593	1239.55
k, conductivity (W/m. K)	0.03392	0.07524	0.05
Pr, Prandtl number	0.8399	0.7237	0.7809

3.3 Design calculations

3.3.1 The total heat transfer rate

$$Q = \dot{m}_{Air} \times c_{pAir} \times \Delta T_{Air} = \dot{m}_{CO_2} \times c_{pCO_2} \times \Delta T_{CO_2} \quad \text{..... [17]}$$

Q= total heat transfer rate

$\dot{m}_{Air}$ =mass flow rate of air

$\dot{m}_{CO_2}$=mass flow rate of CO_2

$c_{p,air}$=specific heat of air under constant pressure

$c_{p,CO2}$= specific heat of CO_2 under constant pressure

ΔT_{Air}= temperature difference in air (between air inlet and outlet)

ΔT_{CO_2}= temperature difference in CO_2 (between CO_2 inlet and outlet)

3.3.2 Logarithmic mean temperature difference

$$\Delta T_{lm} = \frac{\Delta T_1 - \Delta T_2}{Ln(\frac{\Delta T_1}{\Delta T_2})}$$

ΔT_1 = Temperature difference between air and CO_2 at one end of the heat exchanger

ΔT_2= Temperature difference between air and CO_2 at the other end of the heat exchanger

3.3.3 The number of tubes

$$N_t = \frac{\pi}{4}\left(\frac{CTP}{CL}\right)\frac{D_S^2}{PR^2 d_o^2} \quad \text{…….. [29]}$$

CTP=tube count constant (0.93 for one tube pass, 0.9 for two tube passes, 0.85 for three tube passes)

D_s=shell diameter

$Pt = H \times d_o$=tube pitch …… [29]

H=constant (usually 1.25 &1.5)

CL =tube layout constant (1 for '90° & 45°', 0.866 for '30° & 60°')

d_o=Tube outer diameter

$$PR = \frac{Pt}{d_o}$$

3.3.4 The overall heat transfer coefficient

$$U = \frac{1}{\left[\frac{1}{h_i}+\frac{1}{h_o}+\ln\left(\frac{d_o}{d_i}\right)\times\left(\frac{d_i}{2(k_{inc})}\right)\right]} \quad \text{…… [30]}$$

h_i =heat transfer coefficient of CO_2 flowing within tube

h_o =Heat transfer coefficient of air flowing outside tube

d_o =tube outer diameter

d_i =tube inner diameter

k_{inc}=Inconel thermal conductivity

$A_o = \pi \times d_i \times N_t \times L$ =tube external side surface area …… [29]

$A_i = \pi \times d_0 \times N_t \times L$ =tube internal side surface area …… [29]

3.3.5 Reynold number of tube fluid

$$Re_{D,CO_2} = \frac{\dot{m}_{CO_2} \times d_i}{A_c \times \mu_{CO_2}}$$ …… [29]

$\dot{m}_{CO_2}$ =mass flow rate of CO_2

μ_{CO_2} = dynamic viscosity of CO_2

d_i=Inner tube diameter

$$A_c = \frac{\pi}{4} \times \frac{d_1^2 N_t}{N_p}$$ …… [29]

N_p=number of passes

N_t=number of tubes

3.3.6 Friction factor of tube fluid

$$f = (1.58 \times \ln Re_{D,CO_2} - 3.28)^{-2}$$

Re_{D,CO_2} = Reynold number of CO_2 …… [29]

f=friction factor

3.3.7 Nusselt number of tube fluid

$$Nu_{CO_2} = \frac{\frac{f}{2} \times (Re_{D,CO_2} - 1000) \times Pr}{[1 + 12.7\left(\frac{f}{2}\right)^{\frac{1}{2}} \times (Pr)^{\frac{2}{3}} - 1]}$$ ……..…… [29]

f=friction factor

Re_{D,CO_2}=Reynold number of CO_2

Pr_{CO_2}=Prandtl number of CO_2

3.3.8 Heat transfer coefficient of CO_2

$$h_{CO_2} = \frac{Nu_{CO_2} \times k_{CO_2}}{d_i}$$

d_i=Inner tube diameter

k_{CO_2}Thermal conductivity of CO_2

3.3.9 The length of the shell

$$L = \frac{Q}{N_t \times U \times \pi \times d_o \times \Delta T_{lm}} \quad \text{.....[21]}$$

Q= Total heat transfer rate

N_t : Number of tubes

U : Overall heat transfer coefficient;

ΔT_{lm} =logarithmic mean temperature difference

3.3.10 Crossflow area of shell

$$A_s = \frac{D_s \times C_t \times B}{P_t} \quad \text{.....[29]}$$

$B=D_s$= Baffle space .....[29]

$Pt= H \times d_o$=tube pitch .....[29]

H=constant (usually 1.25&1.5)

D_s=shell diameter

$$C_t = P_t - d_o \quad \text{.....[29]}$$

3.3.11 Equivalent diameter

$D_e = 4 \times (Pt^2 - \frac{\pi \times d_o^2}{4})/(\pi \times d_o)$….. Square pitch .....[29]

$Pt= H \times d_o$=tube pitch .....[29]

d_o= Outer tube diameter

3.3.12 Reynold number of air

$$Re_{D,Air} = \frac{\dot{m}_{air} \times D_e}{A_s \times \mu_{Air}} \quad \text{.....[29]}$$

μ_{Air}=dynamic viscosity of air

D_e=equivalent diameter

$$A_s = \frac{D_s \times C_t \times B}{P_t}$$

$\dot{m}_{air}$ = mass flow rate of air

3.3.13 Nusselt number of air

$$Nu_{D,Air} = 0.36 \times Re_{D,Air}^{0.55} \times Pr_{Air}^{\frac{1}{3}} \times (\mu/\mu_w)^{0.14} \quad \text{……..[29]}$$

$Re_{D,Air}$=Reynold number of air

Pr_{Air}=Prandtle number of air

$\mu_w = \mu\ of\ air\ at \ldots\ldots\ldots\ldots\ldots\ldots\ldots\ldots\ T_w$

3.3.14 Heat transfer coefficient of air

$$h_{air} = \frac{Nu_{Air} \times k_{Air}}{D_e}$$

D_e=equivalent diameter

k_{Air}=Air conductivity

3.3.15 Overall heat transfer surface area

$$A_{overall} = \frac{Q}{U \times \Delta T_{lm}} \quad \text{……..[29]}$$

U=Overall heat transfer coefficient

$A_{overall}$=Overall heat transfer surface area

ΔT_{lm}=logarithmic mean temperature difference

$$\Delta T_{lm} = \frac{\Delta T_1 - \Delta T_2}{Ln(\frac{\Delta T_1}{\Delta T_2})}$$

Q=Total heat transfer rate

3.3.16 Shell side pressure drop

$$\Delta p_s = \frac{f G_s^2 (N_b+1)\, D_s}{2\rho_{Air} D_e \times (\mu/\mu_w)^{0.14}} \quad \text{……..[29]}$$

$$f = \exp(0.576 - 0.19 \ln Re_{D,Air}) \quad \text{……..[29]}$$

μ_{Air} = dynamic viscosity of air

D_s=shell diameter

$G_S = \dot{m}_{Air} / A_S$

$\dot{m}_{air}$ = mass flow rate of air

$$A_s = \frac{D_s \times C_t \times B}{P_t}$$

N_b= number of baffles

$\mu_w = \mu\ at \ldots\ldots\ldots\ldots\ldots\ldots\ldots\ldots\ T_w$

$$T_w = \frac{1}{2}\left[\frac{T_{ci}+T_{co}}{2} + \frac{T_{hi}+T_{ho}}{2}\right] \qquad \text{……..[29]}$$

3.3.17 Tube side pressure drop

$$\Delta p_f = 4\left[\frac{f \times L}{d_1} + 1\right] \times N_p \times \rho_{CO_2} \frac{\mu_{CO_2}^2}{2} \qquad \text{……..[29]}$$

$$f = (1.58 \times \ln Re_{D,CO_2} - 3.28)^{-2} \qquad \text{……..[29]}$$

N_p=number of passes

L=length of shell

d_i =tube inner diameter

ρ_{CO_2}=density of CO_2

μ_{CO_2} = dynamic viscosity of CO_2

3.3.18 Shell thickness

$$t_s = \frac{pD_s}{f_c \times J - 0.6p} + c \qquad \text{……..[14]}$$

t_s=shell thickness

p=design pressure

f_c= maximum allowable stress of the material of construction

J=Joint efficiency (varies from 0.7 to 0.9)

D_s=shell diameter

c=corrosion allowance

3.3.19 Tube thickness

$$t_t = \frac{pd_o}{2(f_c \times J + 0.4p)} \quad \text{……..[14]}$$

t_t= tube thickness

d_o =tube outer diameter

f_c= maximum allowable stress of the material of construction

J=Joint efficiency (varies from 0.7 to 0.9)

p=design pressure

4 PRELIMINARY DESIGN AND OPTIMIZATION USING EMPIRICAL EQUATION

The preliminary design of the S-CO_2 heat exchanger was conducted using empirical equations 3.3.1 to 3.3.19. The inner tube diameter selected varies from 0.028 m to 0.13 m. The shell diameter selected varies from 4 m to 18 m. Other constant parameters are specified in table 3.4 and 3.5 Also, the tube is one pass at initial set of $Pt = 1.5 \times d_o$& $B = 1.7 \times D_s$

4.1 Effect of shell inner diameter on the design and performance parameters $\boldsymbol{d_i}$=0.0092 m, $\boldsymbol{D_s}$,=6-18 m $\boldsymbol{t_t}$=0.004 m

Table 4.1 shows the effect of shell diameter on design details of the heat exchanger when the tube inner diameter is set as 0.092 m. The values presented shows that the number of tubes, tube internal side surface area, tube external side surface area, volume of shell material, total volume of tube material, overall surface area and mass of material increases as the shell diameter increases. This is due to increase in cross sectional area [37]. However, the shell length, the number of baffles, overall heat transfer coefficient, the shell side pressure drop and tube side pressure drop all decreases as shell diameter increases, this is attributed to a reduced velocity caused by the increased total cross section area of tubes and baffle space [38]. These relations are presented in Figures 4.1 (a) to 4.1 (e). Smaller shell diameters are preferred as they offer fewer tube numbers, moderate shell and tube side pressure drop, reduced mass of heat exchanger material and a better overall heat transfer coefficient. This is seen in Table 4.1 for shell diameter 6 m and 18 m.

Table 4. 1: Effect of shell inner diameter on the design and performance parameters $\mathbf{d_i}$=0.0092 m, $\mathbf{D_s}$,=6-18 m $\mathbf{t_t}$=0.004 m

Parameters	Data						
Shell Outer diameter (m)	6.11	8.15	10.19	12.23	14.26	16.31	18.34
Shell Inner diameter (m)	6	8	10	12	14	16	18
Shell Side Pressure drop (Bar)	7.76	2.26	0.87	0.40	0.21	0.12	0.07
Shell length (m)	36.67	30.25	26.10	23.16	20.96	19.23	17.85
Surface Area of Inner Shell (m^2)	691.30	760.36	820.06	873.22	921.99	966.73	1,009.52
Volume of Shell material (m^3)	39.43	57.56	77.81	99.16	120.97	151.29	173.24
Tube number	1,682	2,992	4,675	6,732	9,162	11,967	15,146
Tube Side Pressure drop (Pa)	364.04	110.05	43.72	20.63	10.96	6.35	3.93
Volume of tube material (m^3)	0.04	0.04	0.03	0.03	0.03	0.02	0.02
Total volume of tubes material (m^3)	74.42	109.20	147.22	188.11	231.70	277.65	326.19
Total length of tubes (m)	61,679	90,508	122,018	155,913	192,036	230,125	270,356
Tube internal side surface area (m^2)	17,829	26,163	35,271	45,069	55,511	66,521	78,150
Tube external side surface area (m^2)	19,380	28,438	38,338	48,988	60,338	72,305	84,946
Baffle number	8	5	3	2	1	1	1
Overall heat transfer coefficient (W/m^2K)	84.02	57.31	42.51	33.26	27.00	22.53	19.18
Overall Area (m^2)	17,899	26,240	35,379	45,215	55,686	66,751	78,387
Mass of material (kg)	951,734	1,394,133	1,881,234	2,401,596	2,948,302	3,586,002	4,175,253

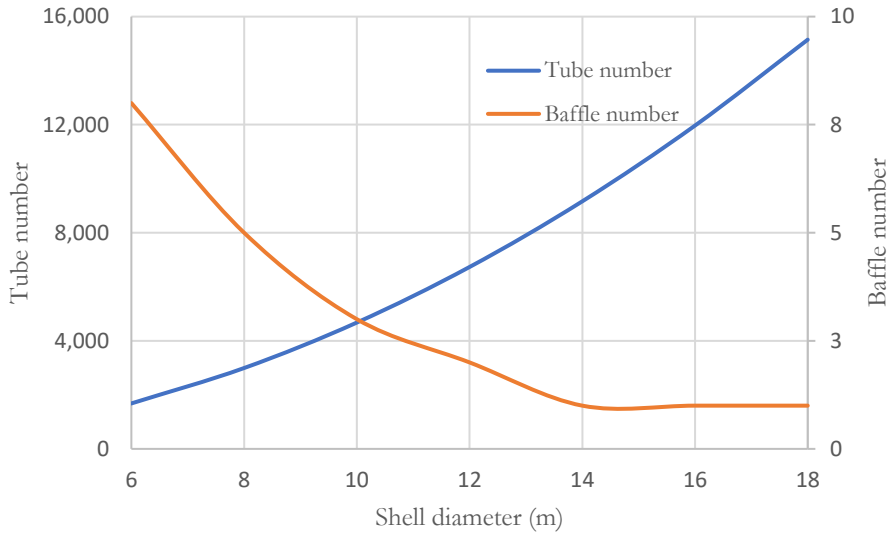

(a) Tube number and baffle number

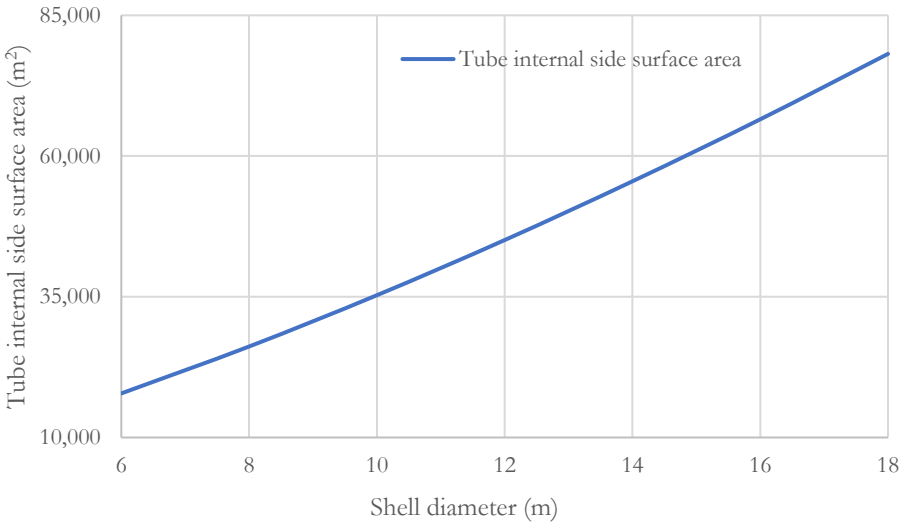

(b) Total tube internal side surface area

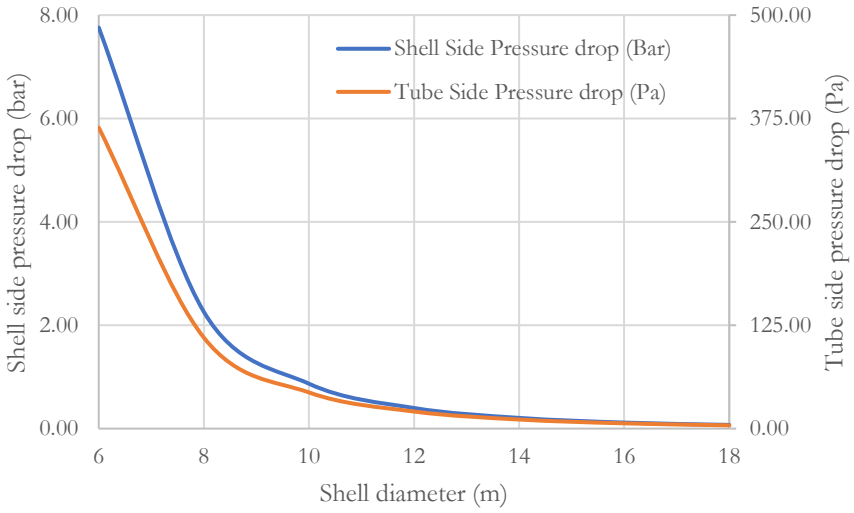

(c) shell side pressure drop and tube side pressure drop

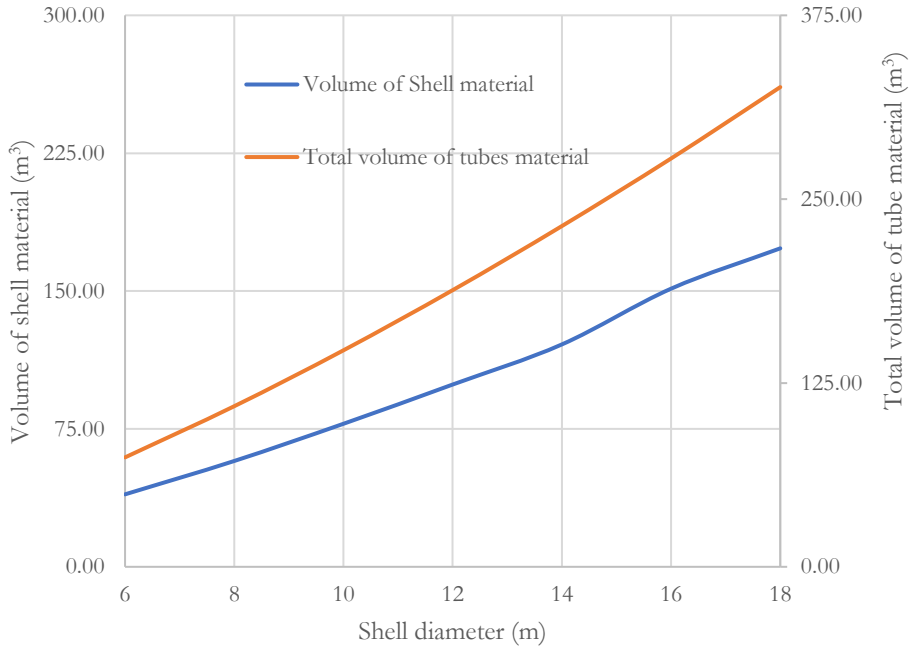

(d) volume of shell and total volume of tubes materials

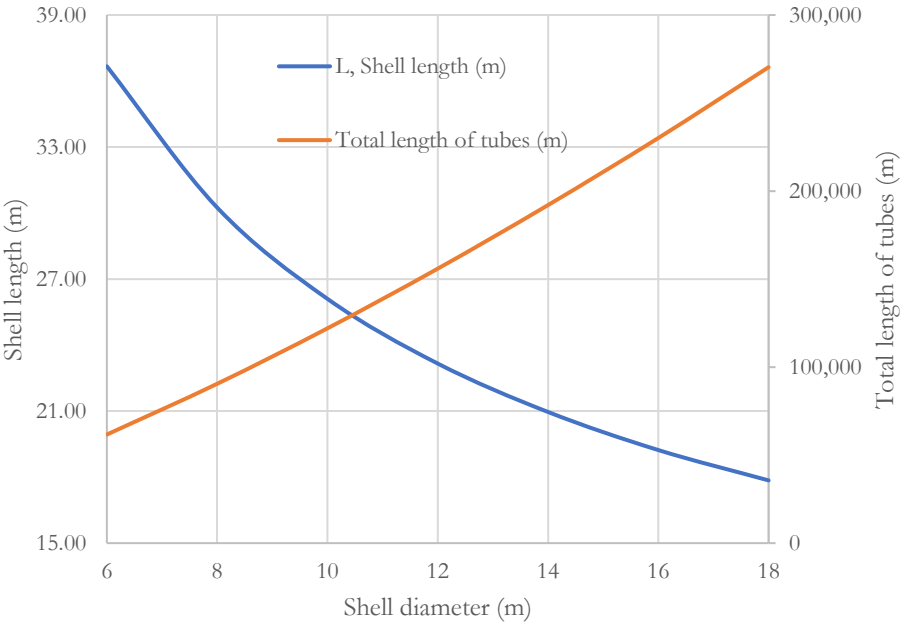

(e) Shell length and total length of tubes

Figure 4. 1: Effect of shell inner diameter on the design and performance parameters $\mathbf{d_i}$=0.0092 m, $\mathbf{D_s}$,=6-18 m $\mathbf{t_t}$=0.004 m

4.2 Effect of inner tube diameter on the design and performance parameters, $\mathbf{D_s}$=8m, $\mathbf{d_i}$=0.028 – 0.120 m $\mathbf{t_s}$. =0.075 m

Table 4.2 shows the effect of inner tube diameter on the key design parameters which include the number of baffles, number of tubes, total surface area of shell, total surface area of tubes, volume of shell, total volume of tubes, shell length, the shell side pressure drop and tube side pressure drop when shell diameter is kept as 8m. Increasing the tube diameter increases the shell length, volume of tube, number of baffles, shell side pressure drop, tube side pressure drop, overall surface area of device, heat transfer area of inside tubes and heat transfer area of outside tubes. The overall heat transfer coefficient, total length of tubes and number of tubes decreases as tube diameter increases. These relations are presented in figures 4.2 (a) to (e). A tube diameter increase lead to decrease in the number of tubes arranged in the shell because the shell can accommodate less number of larger tubes than smaller one. The number of baffles is directly proportional to shell length. This is so because the number of baffles is a division of shell length by baffle space. It is important to also note that the total heat transfer coefficient increases as the tube diameter decreases, this is because of the increase in number of tubes arranged in the shell resulting in higher collision of the particles of the fluid moving round the tubes.

Table 4. 2: Effect of inner tube diameter on the design and performance parameters, D_s=8m, d_i=0.028 – 0.120 m t_s. =0.075 m

Parameters	Data					
Tube Outer diameter (m)	0.030	0.050	0.070	0.090	0.110	0.130
Tube Inner diameter (m)	0.028	0.046	0.065	0.083	0.102	0.120
Shell Side Pressure drop (Bar)	1.92	2.05	2.15	2.23	2.29	2.35
Shell length (m)	6.12	12.03	18.81	26.29	34.34	42.91
Surface Area of Inner Shell (m^2)	153.78	302.39	472.81	660.83	863.17	1078.69
Volume of Shell material (m^3)	11.64	22.89	35.79	50.03	65.34	81.66
Tube number	33,242	11,967	6,106	3,694	2,473	1,770
Tube Side Pressure drop (Pa)	102.39	105.17	107.38	109.22	110.83	112.26
Volume of tube material (m^3)	0.0005575	0.0036286	0.0107392	0.0250081	0.0484926	0.0842724
Total volume of tubes (m^3)	18.53	43.42	65.57	92.38	119.92	149.16
Total length of tubes (m)	203,371	143,963	114,854	97,115	84,923	75,958
Tubes total internal side surface area (m^2)	17,892	20,807	23,312	25,326	27,083	28,639
Tubes total external side surface area (m^2)	19,170	22,617	25,261	27,462	29,351	31,026
Baffle number	0	1	2	4	5	7
Overall heat transfer coefficient (W/m^2K)	84.99	72.01	64.48	59.35	55.52	52.51
Overall Area (m^2)	17,693	20,882	23,320	25,339	27,086	28,640
Mass of material (kg)	252,241	554,397	847,427	1,190,519	1,548,832	1,929,672

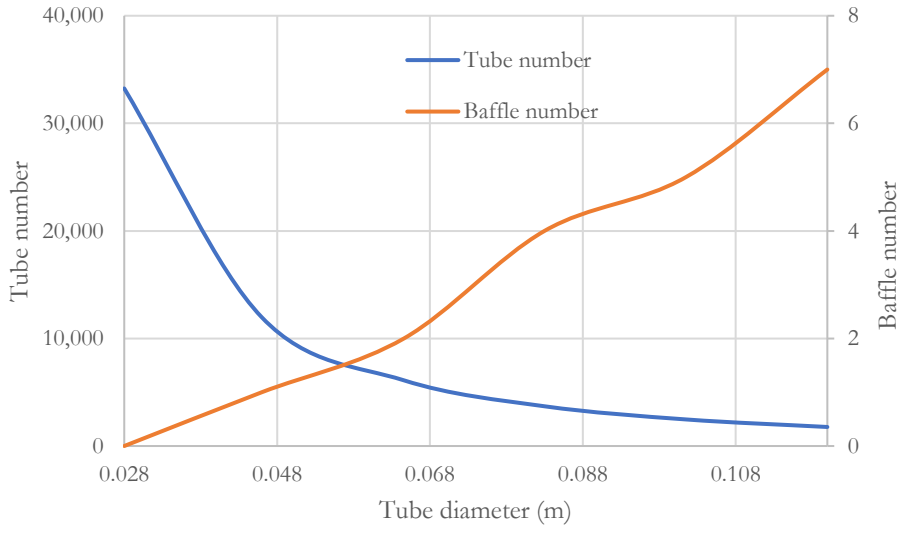

(a) Tube number and baffle number

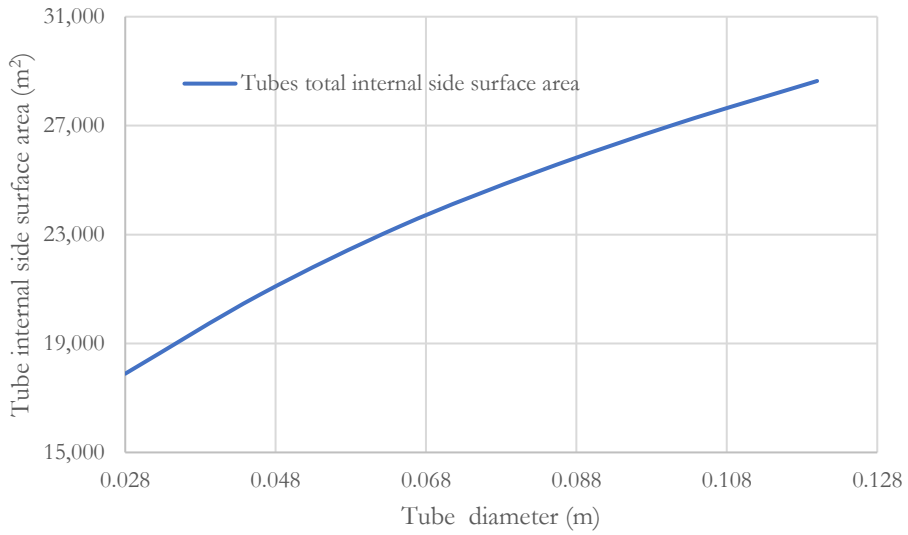

(b)Tubes total internal surface area

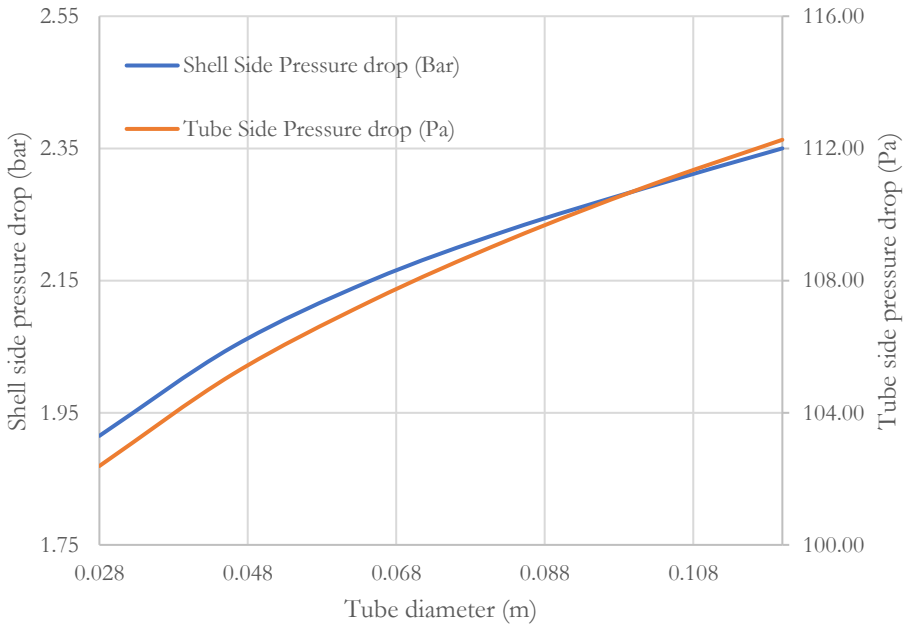

(c) Shell side pressure drop and tube side pressure drop

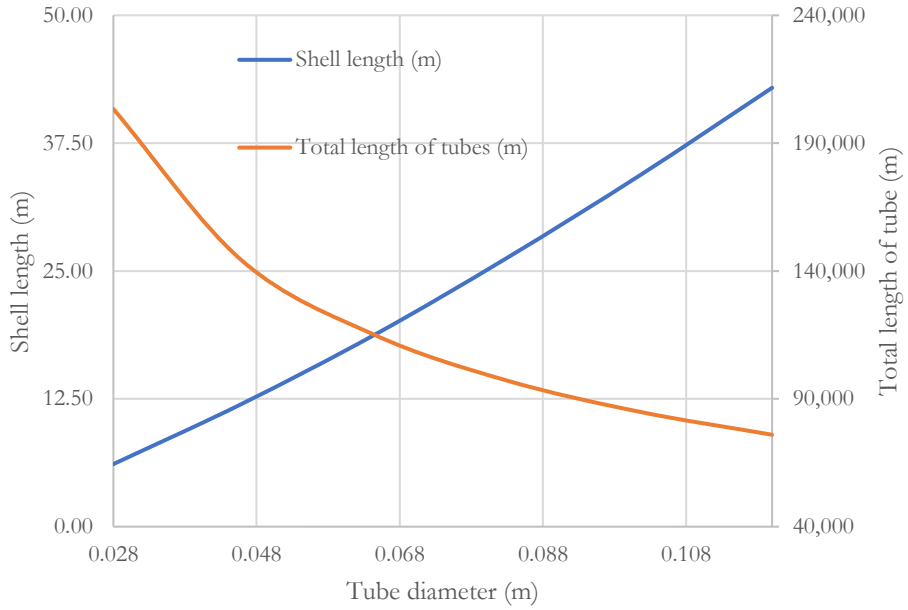

(d) Shell length and total length of tubes

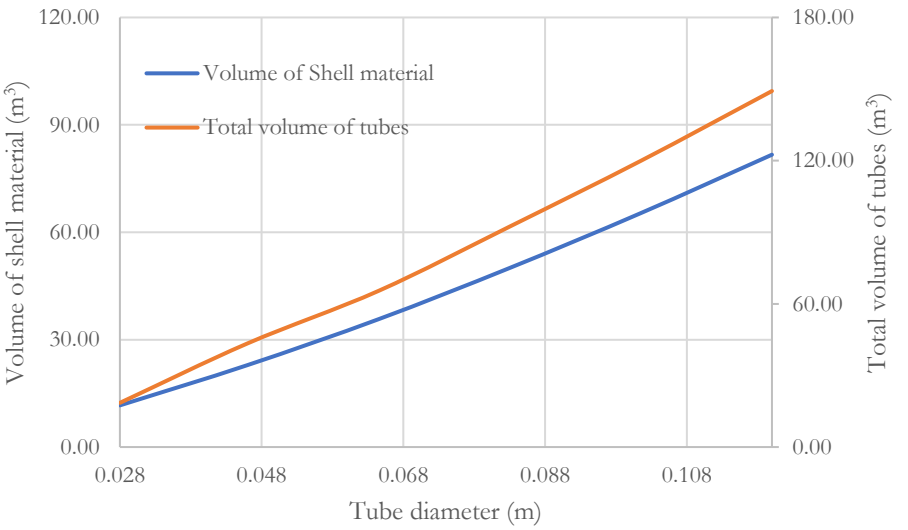

(e)Volume of shell and total volume of tubes

Figure 4. 2: Effect of inner tube diameter on the design and performance parameters, $\boldsymbol{D_s}$=8m, $\boldsymbol{d_i}$=0.028 – 0.120 m $\boldsymbol{t_s}$. =0.075 m

4.3 Effect of tube and shell diameter on the design and performance parameters, D_s, =4-16 m

d_i=0.05, 0.09 & 0.13 m.

The combined effects of tube diameter and shell diameter have been checked against tube number, shell length, volume of tube material, volume of shell material, shell side pressure drop, tube side pressure drop, total surface area for heat transfer, and overall heat transfer coefficient.

Table 4.3 and Figure 4.3 show the effect of tube and shell diameter on tube numbers. The tube number increases with the increased shell diameter and decreased tube diameter. This signifies that more tubes are required to fill a shell diameter space for smaller tube diameters as compared to larger tubes.

Table 4. 3: Effect of tube and shell diameter on tube number

Parameter	Data						
Shell Outer diameter (m)	4.08	6.11	8.15	10.19	12.23	14.26	16.30
Shell Inner diameter (m)	4	6	8	10	12	14	16
Tube number d_i = 0.05 m	2,992	6,732	11,967	18,699	26,926	36,649	47,868
Tube number d_i = 0.09 m	923	2,078	3,694	5,771	8,310	11,311	14,774
Tube number d_i = 0.13 m	443	996	1,770	2,766	3,983	5,422	7,081

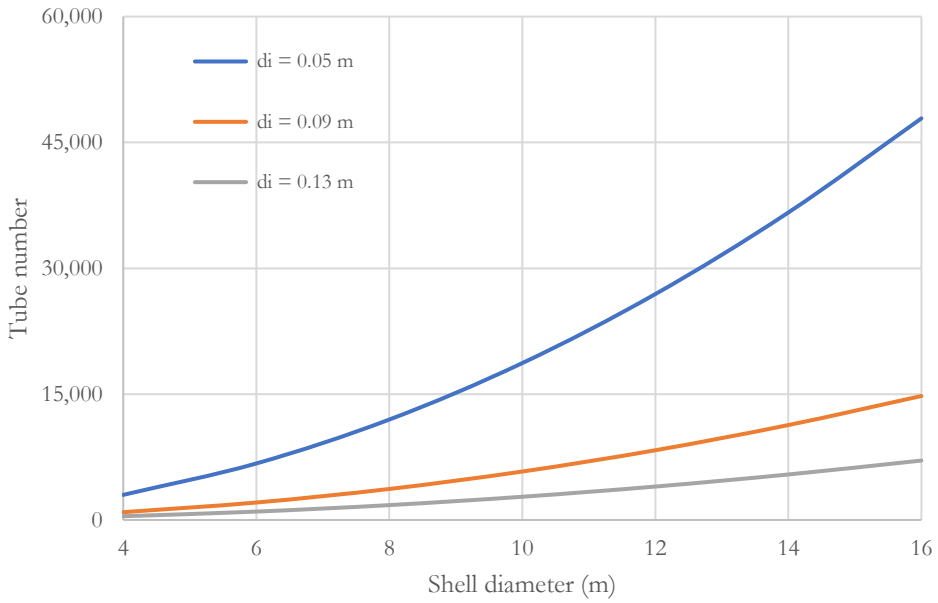

Figure 4. 3: Effect of tube and shell diameter on tube number

4.4 Effect of tube and shell diameter on shell length

Table 4.4 and Figure 4.4 shows the effect of shell and tube diameter on the length of shell needed for this heat exchanger to achieve the heat transfer needed. As expected, decreasing the tube diameter decreases the length needed for the same shell diameter. Decreasing tube diameter from 0.13 m to 0.05 m at 8m shell diameter decreased the shell length from 60.18 m to 16.35 m, which is 72.83% of the shell length observed at tube diameter of 0.13 m. This is due to the increased surface area/volume ratio of the smaller tube compared to the large one as shown in Table 4.5 and Figure 4.5. In comparison, increasing shell diameter also decreases the length of the heat exchanger but at relatively less scale. For example, the shell length observed at 16 m shell diameter and 0.13 m tube diameter is 36.46 m which is 63.05% of the 60.18 m shell length derived at shell diameter of 8 m. It is evident that decreasing shell diameter is more effective in reducing shell length

Table 4. 4: Effect of tube and shell diameter on shell length, m

Parameter	Data						
Shell Outer diameter (m)	4.08	6.11	8.15	10.19	12.23	14.26	16.30
Shell Inner diameter (m)	4	6	8	10	12	14	16
Shell length (m) d_i = 0.05 m	27.15	20.14	16.35	13.95	12.26	11.02	10.06
Shell length (m) d_i = 0.09 m	60.94	44.95	36.42	30.98	27.18	24.36	22.19
Shell length (m) d_i = 0.13 m	101.30	74.45	60.18	51.12	44.80	40.10	36.46

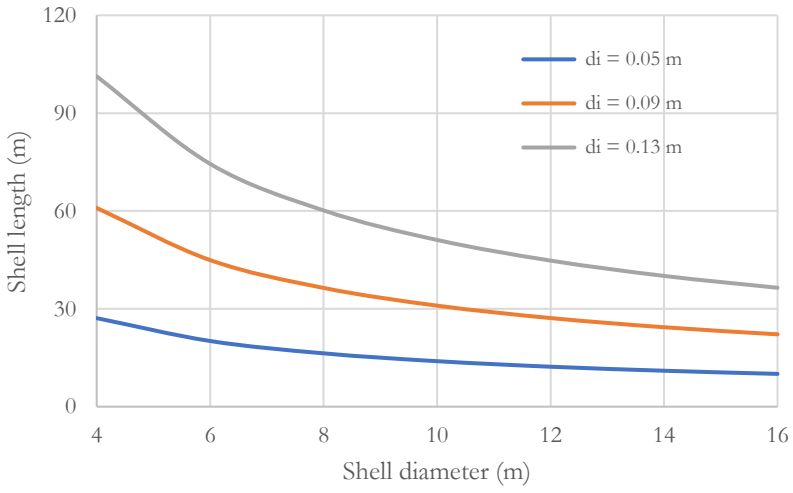

Figure 4. 4: Effect of tube and shell diameter on shell length, m

Table 4. 5: Effect of tube diameter on surface area to volume ratio, m

Tube Outer diameter (m)	0.010	0.030	0.050	0.070	0.090	0.110	0.130
Tube Inner diameter (m)	0.009	0.028	0.046	0.065	0.083	0.102	0.120
Side surface area to volume ratio of tube (m^{-1})	2496	832	499.2	356.57	277.33	226.91	192

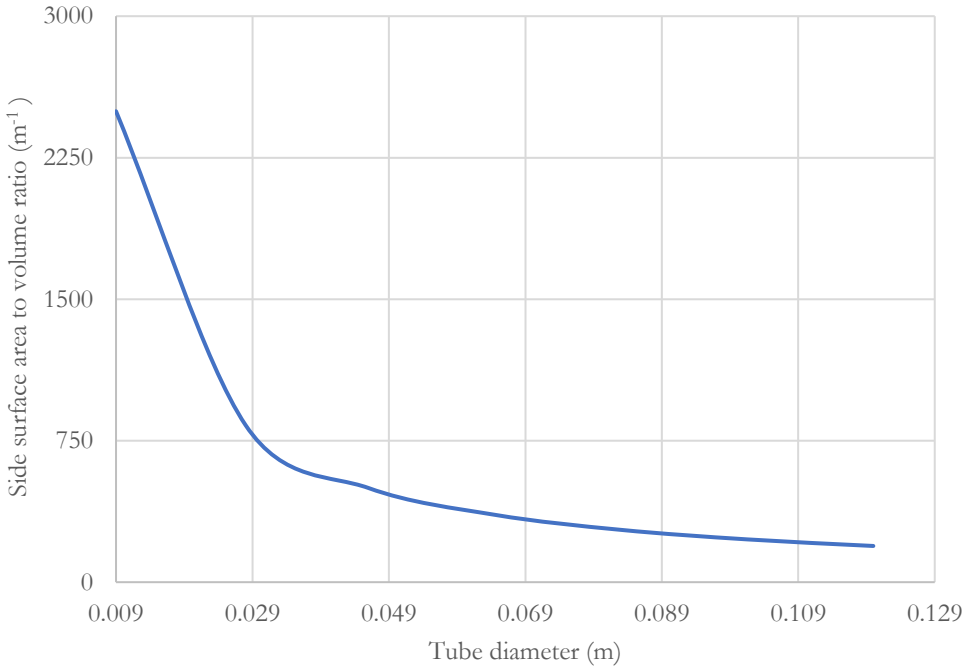

Figure 4. 5: Effect of tube diameter on side surface area to volume ratio.

4.5 Effect of tube and shell diameter on total volume of tube material, m^3

As shown in Table 4.6 and Figure 4.6, the total volume of tube material decreases significantly with the decreasing shell diameter for tube diameter 0.13 m when compared to tube diameter 0.09 m and 0.05 m. For bigger tubes, the decrease in volume of tube material is sharply noticed while for smaller tubes, the changes is relatively small . Decreasing the diameter of the tube decreases the total volume of tube material due to the increased surface area for heat transfer and reduced tube thickness from 5.00 mm to 1.90 mm. The heat exchanger should be designed as small shell diameter, with small tubes.

Table 4. 6: Effect of tube and shell diameter on total volume of tube material, m^3

Parameter	Data						
Shell Outer diameter (m)	4.08	6.11	8.15	10.19	12.23	14.26	16.30
Shell Inner diameter (m)	4	6	8	10	12	14	16
Total volume of tube material (m^3) d_i = 0.05 m	23.59	39.38	56.85	75.75	95.92	117.28	139.85
Total volume of tube material(m^3) d_i = 0.09 m	52.96	87.96	126.60	168.27	212.58	259.30	308.27
Total volume of tube material (m^3) d_i = 0.13 m	88.04	145.68	209.22	277.68	350.38	426.92	506.97

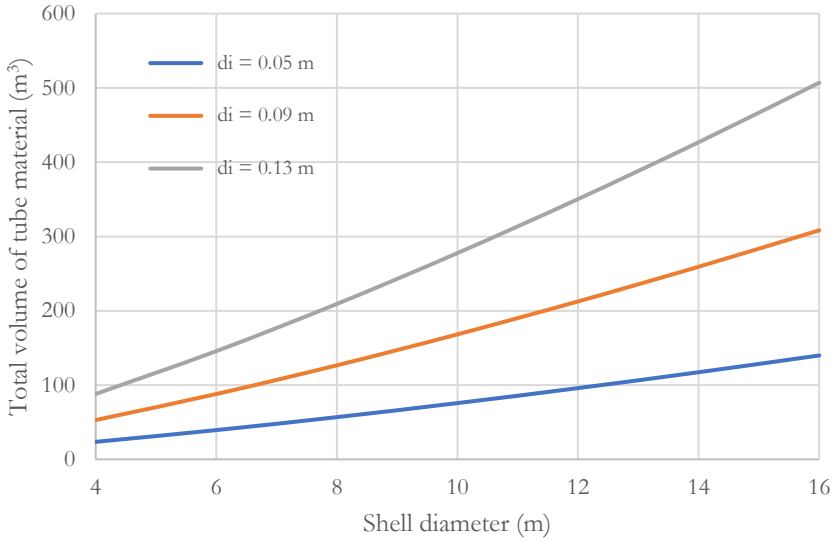

Figure 4. 6: Effect of tube and shell diameter on total volume of tube material, m^3

4.6 Effect of tube and shell diameter on volume of shell material

In Table 4.7 and Figure 4.7, the volume of shell materials increases significantly for tube diameter 0.05 m, 0.09 m and 0.13 m at about same proportion. This is to further buttress the observation from figure 4.1 and figure 4.2. It is seen that at shell diameter 6 m, a decrease in volume of shell material by 72.96 % when tube diameter was reduced from 0.13 m to 0.05 m. A decrease in volume of shell material by 48.0 % is seen at tube diameter 0.05 m when shell diameter decreases from 10 m to 6 m. A conclusion that reduction in tube diameter helps greatly in decreasing the amount of shell material is noticed.

Table 4. 7: Effect of tube and shell diameter on volume of shell material, m^3

Parameter	Data						
Shell Outer diameter (m)	4.08	6.11	8.15	10.19	12.23	14.26	16.30
Shell Inner diameter (m)	4	6	8	10	12	14	16
Volume of Shell material (m^3) d_i = 0.05 m	12.58	21.63	31.22	41.60	52.67	64.40	76.79
Volume of Shell material (m^3) d_i = 0.09 m	28.08	48.30	69.52	92.40	116.73	142.38	169.28
Volume of Shell material (m^3) d_i = 0.13 m	48.35	79.99	114.88	152.47	192.40	234.43	278.38

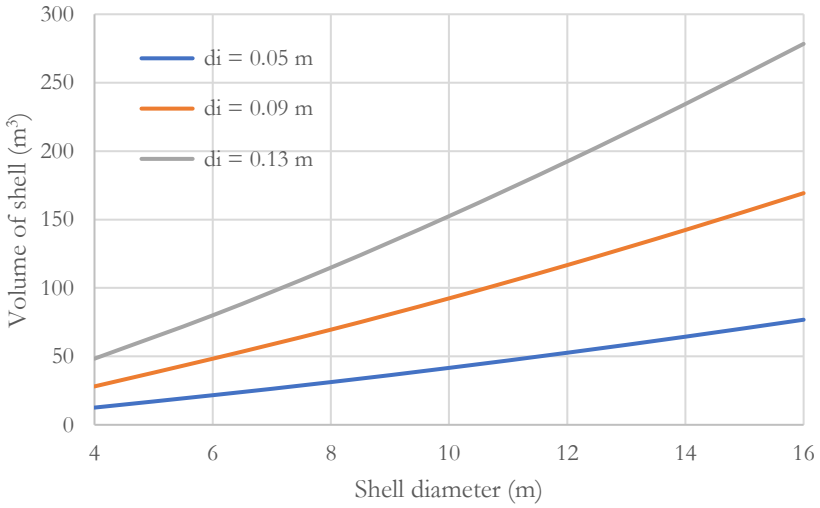

Figure 4. 7: Effect of tube and shell diameter on volume of shell material, m^3

4.7 Effect of tube and shell diameter on tube side pressure drop

Table 4.8 and Figure 4.8 shows the effect of tube diameter and shell diameter on pressure drop of CO_2 flowing in the tube. As expected, increasing shell diameter decreases the pressure drop as more tubes are used which decrease the velocity of CO_2 and length of tube (shell) . In comparison, the effect of tube diameter on pressure drop is negligible with the range of tube diameter examined. It should be noted that the pressure drop in tube is very small compared to the 10 MPa working pressure of CO_2 in tube.

Table 4. 8: Effect of tube and shell diameter on tube side pressure drop, Pa

Parameter	Data						
Shell Outer diameter (m)	4.08	6.11	8.15	10.19	12.23	14.26	16.30
Shell Inner diameter (m)	4	6	8	10	12	14	16
Tube Side Pressure drop (Pa) d_i = 0.05 m	2,341.58	422.00	126.62	50.03	23.53	12.47	7.22
Tube Side Pressure drop (Pa) d_i = 0.09 m	2,529.05	450.34	133.82	52.52	24.55	12.94	7.45
Tube Side Pressure drop (Pa) d_i = 0.13 m	2,668.00	470.95	139.16	54.38	25.33	13.32	7.64

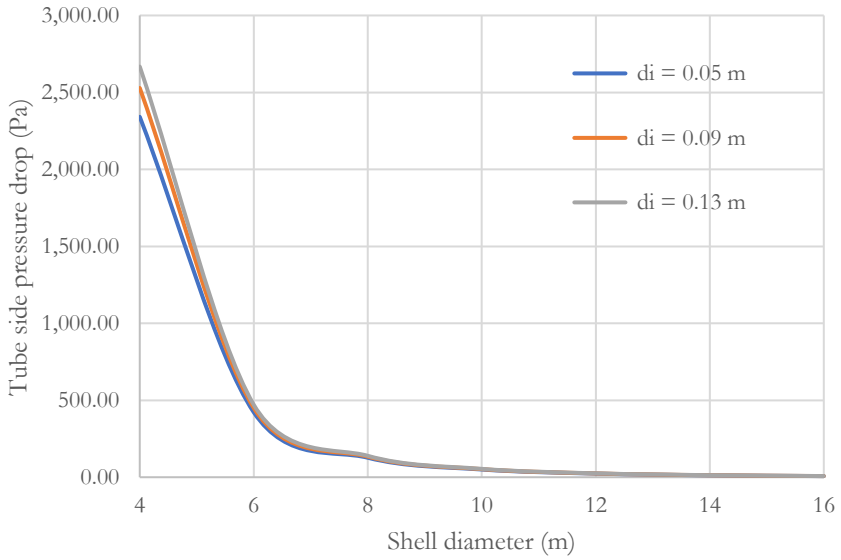

Figure 4. 8: Effect of tube and shell diameter on tube side pressure drop, Pa

4.8 Effect of tube and shell diameter on shell side pressure drop

Table 4.9 and Figure 4.9 shows the effect of tube and shell diameters on the pressure drop in shell side. It is evident that the pressure drop in shell side is dominated by shell diameter. Increasing shell diameter increases the cross-section area and decrease the velocity of air. Table 4.10 and Figure 4.10 shows the effect of shell and tube diameter on the velocity of air in shell examined. The changes in velocity is dominated by the shell diameter. The decreased shell length at large shell diameter also linearly decreases the pressure drop in shell side. It was observed that shell side pressure drops had a major decrease as shell diameter increased from 4 m to 16 m showing that low shell side pressure drop

is achieved as shell diameter increases. This is in further compliance with the observations of session 4.1 and 4.2

Table 4. 9: Effect of tube and shell diameter on shell side pressure drop, bar

Parameter	Data						
Shell Outer diameter (m)	4.08	6.11	8.15	10.19	12.23	14.26	16.30
Shell Inner diameter (m)	4	6	8	10	12	14	16
Shell Side Pressure drop (Bar) d_i = 0.05 m	10.120	1.730	0.496	0.189	0.085	0.044	0.025
Shell Side Pressure drop (Bar) d_i = 0.09 m	11.289	1.920	0.548	0.208	0.094	0.048	0.027
Shell Side Pressure drop (Bar) d_i = 0.13 m	12.120	2.050	0.585	0.222	0.100	0.051	0.029

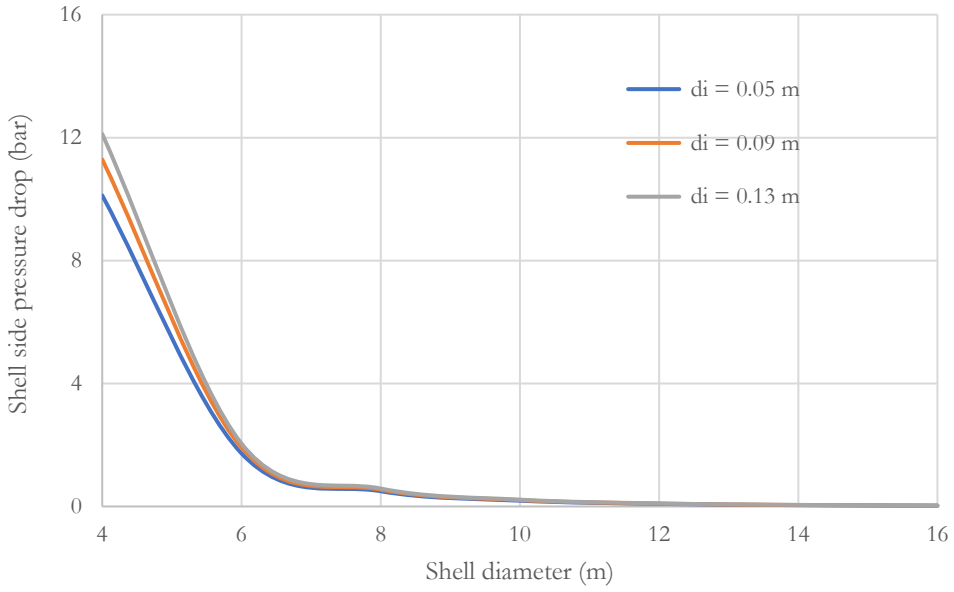

Figure 4. 9: Effect of tube and shell diameter on shell side pressure drop, bar

Table 4. 10: Effect of shell and tube diameter on the velocity of air, m/s

Parameter	Data						
Shell Outer diameter (m)	4.08	6.11	8.15	10.19	12.23	14.26	16.30
Shell Inner diameter (m)	4	6	8	10	12	14	16
Velocity of Air (m/s) d_i = 0.05 m	448.34	199.26	112.09	71.74	49.82	36.60	28.02
Velocity of Air (m/s) d_i = 0.09 m	448.34	199.26	112.09	71.74	49.82	36.60	28.02
Velocity of Air (m/s) d_i = 0.13 m	448.34	199.26	112.09	71.74	49.82	36.60	28.02

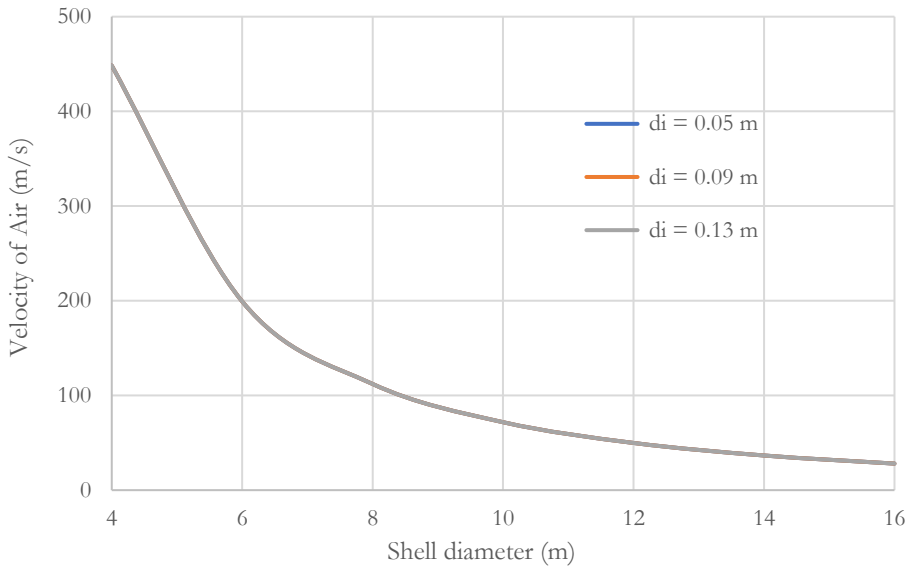

Figure 4. 10: Effect of shell and tube diameter on the velocity of air, m/s

4.10 Effect of tube and shell diameter on overall heat transfer coefficient

Table 4.11 and Figure 4.11 presents the effect of tube and shell diameter on overall heat transfer coefficient. The overall heat transfer coefficient decreases as shell diameter and tube diameter increases. It is noticed at shell diameter 6 m, the heat transfer coefficient dropped by 29.71% from tube diameter 0.05 m to 0.13 m whereas at tube diameter 0.05 m a drop of 48.01% was observed from shell diameter 6 m to 10 m. It is evident that the variation in shell diameter has a higher effect on overall heat transfer coefficient compared to the change in tube diameter.

Table 4. 11: Effect of tube and shell diameter on overall heat transfer coefficient, W/m^2K

Parameter	Data						
Shell Outer diameter (m)	4.08	6.11	8.15	10.19	12.23	14.26	16.30
Shell Inner diameter (m)	4	6	8	10	12	14	16
Overall heat transfer coefficient (W/m^2K) d_i = 0.05 m	127.70	76.50	52.98	39.77	31.41	25.69	21.54
Overall heat transfer coefficient (W/m^2K) d_i = 0.09 m	102.39	61.65	42.84	32.23	25.51	20.91	17.59
Overall heat transfer coefficient (W/m^2K) d_i = 0.13 m	88.97	53.77	37.44	28.21	22.36	18.34	15.45

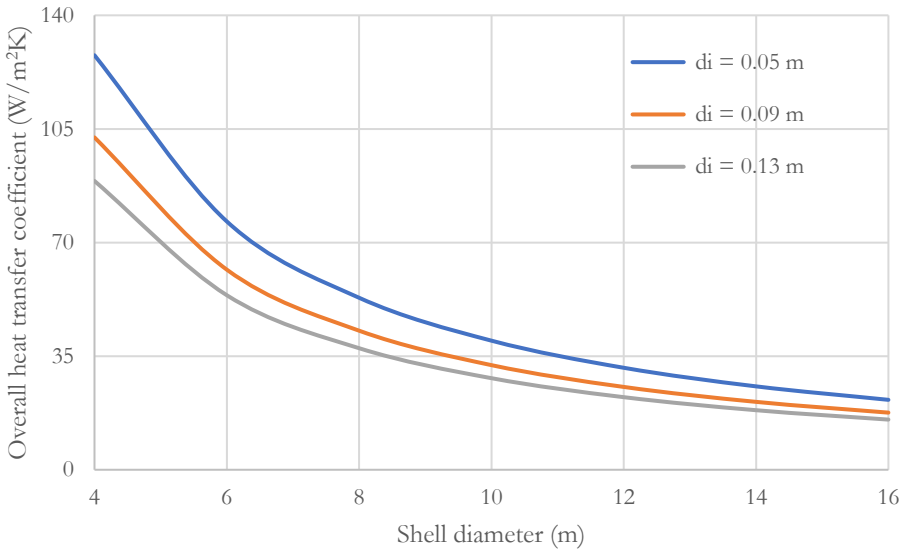

Figure 4. 11: Effect of tube and shell diameter on overall heat transfer coefficient, W/m^{2}K

4.11 Effect of tube and shell diameter tube internal side surface area

Table 4.12 and Figure 4.12 presents the effect of tube and shell diameter on tube internal side surface area. The tube internal side surface area increases as shell diameter and tube diameter increases. It is noticed at shell diameter 6 m, the tube internal side surface area is increased by 42.69 % when tube diameter is increased from 0.05 m to 0.13 m. In comparison, at tube diameter 0.05 m, a huge increase of 92.93 % was observed when shell diameter was increased from 6 m to 10 m. Variation in shell diameter has a higher effect on tube internal side surface area compared to variation of tube diameter dimensions.

Table 4. 12: Effect of tube and shell diameter tube internal side surface area, m^2

Parameter	Data						
D_s, Shell Outer diameter (m)	4.08	6.11	8.15	10.19	12.23	14.26	16.30
D_s, Shell Inner diameter (m)	4	6	8	10	12	14	16
Tube internal side surface area(m^2) d_i = 0.05 m	11,778	19,600	28,383	37,814	47,880	58,549	69,811
Tube internal side surface area(m^2) d_i = 0.09 m	14,689	24,394	35,110	46,666	58,956	71,912	85,492
Tube internal side surface area(m^2) d_i = 0.13 m	16,905	27,969	40,170	53,313	67,274	81,969	97,339

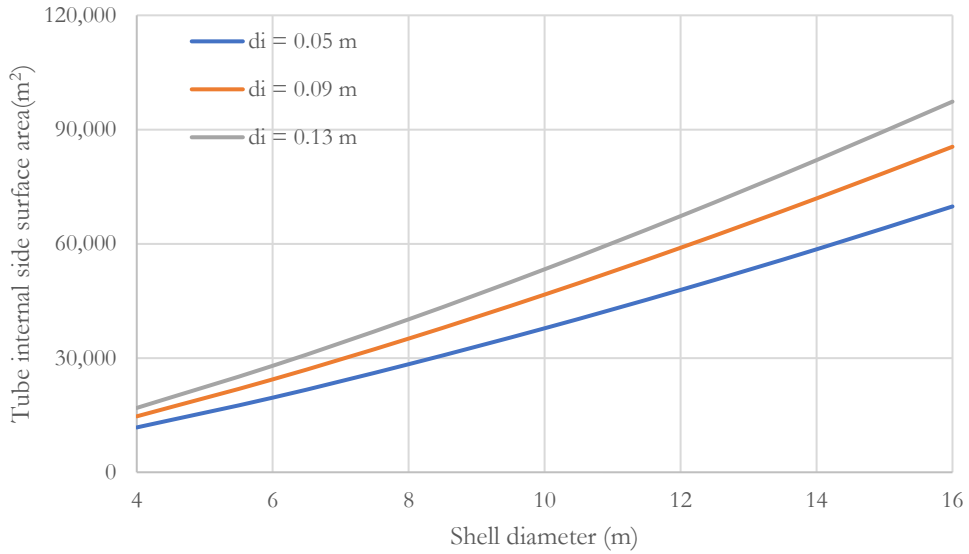

Figure 4. 12: Effect of tube and shell diameter on tube internal side surface area, m^2

4.12 Effect of Tube pitch on shell and tube side pressure drop $\boldsymbol{D_s = 8\ m}$, $\boldsymbol{d_i = 0.102}$,$\boldsymbol{B = 5.6\ m}$, $\boldsymbol{Pt = 1.2 - 2.0}$

The effect of tube pitch on shell and tube side pressure drop is shown in Table 4.13 and Figure 4.13. The shell side pressure drop decreases with the increase in pitch as it increases the cross section area for air to flow through. However, increasing tube pitch increases the pressure drop in tube as the number of tubes is decreased while shell diameter is kept as constant. The highest shell side pressure drop, 17.70 bar was noticed when the tube pitch was 1.2. The lowest shell side pressure drop, 1.17 bar was observed at a tube pitch of 2.0.

Table 4. 13: Effect of Tube pitch on shell and tube side pressure drop

Parameters	Data						
Tube Pitch	2.00× d_o	1.80× d_o	1.60× d_o	1.50× d_o	1.35× d_o	1.25× d_o	1.20× d_o
Shell Side Pressure drop (Bar)	1.17	1.49	2.17	2.88	5.40	10.60	17.10
Tube Side Pressure drop (Pa)	1324.00	708.64	360.92	252.41	143.56	96.55	78.63

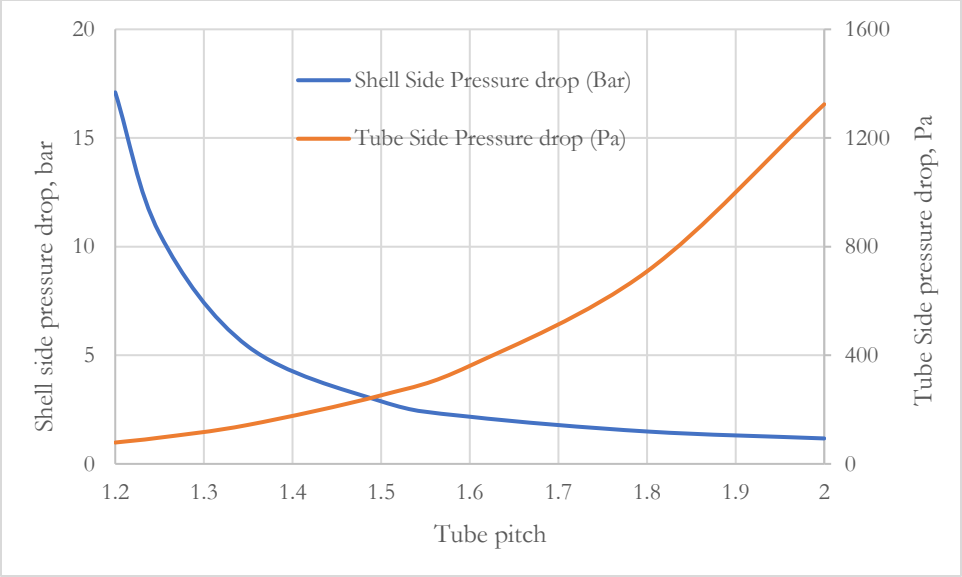

Figure 4. 13: Effect of Tube pitch on shell and tube side pressure drop

The effect of tube pitch on shell length is shown in Table 4.14 and Figure 4.14. Increasing tube pitch increases the length of shell. This is mainly due to the decreased number of tubes when tube pitch is increased when shell diameter is kept constant as shown in Table 4.15 and Figure 4.15. More space is created around the tubes when tube pitch increases, this result in reduced space available for tubes to fit in.

Table 4. 14: Effect of Tube pitch on shell length

Parameters	**Data**						
Tube Pitch	2.00× d_o	1.80× d_o	1.60× d_o	1.50× d_o	1.35× d_o	1.25× d_o	1.20× d_o
Shell length (m)	98.99	72.46	51.62	43.13	32.57	26.84	24.35

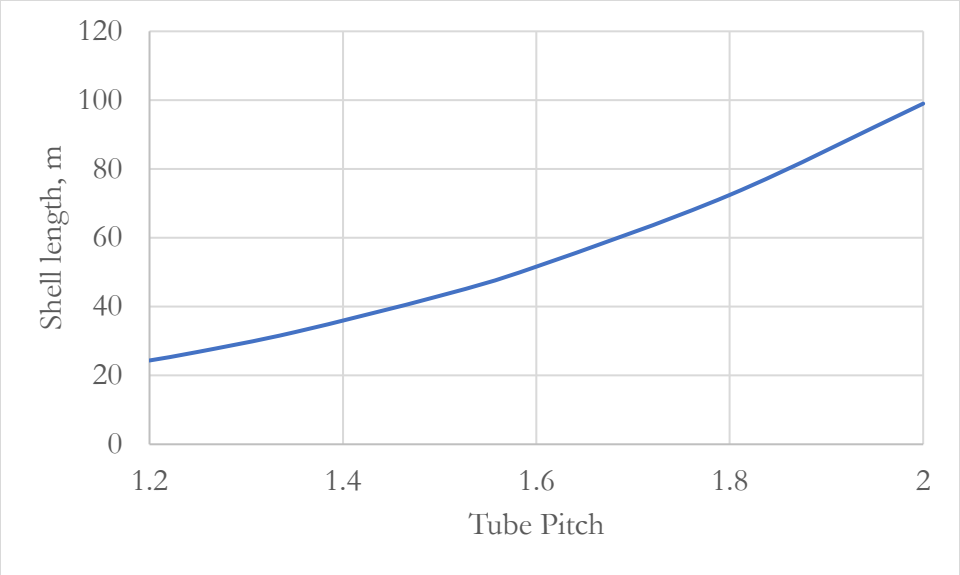

Figure 4. 14: Effect of Tube pitch on shell length

Table 4. 15: Effect of Tube pitch on Tube number

Parameters	Data						
Tube Pitch	2.00 × d_o	1.80× d_o	1.60× d_o	1.50× d_o	1.35× d_o	1.25× d_o	1.20× d_o
Tube number	956	1192	1509	1717	2120	2473	2683

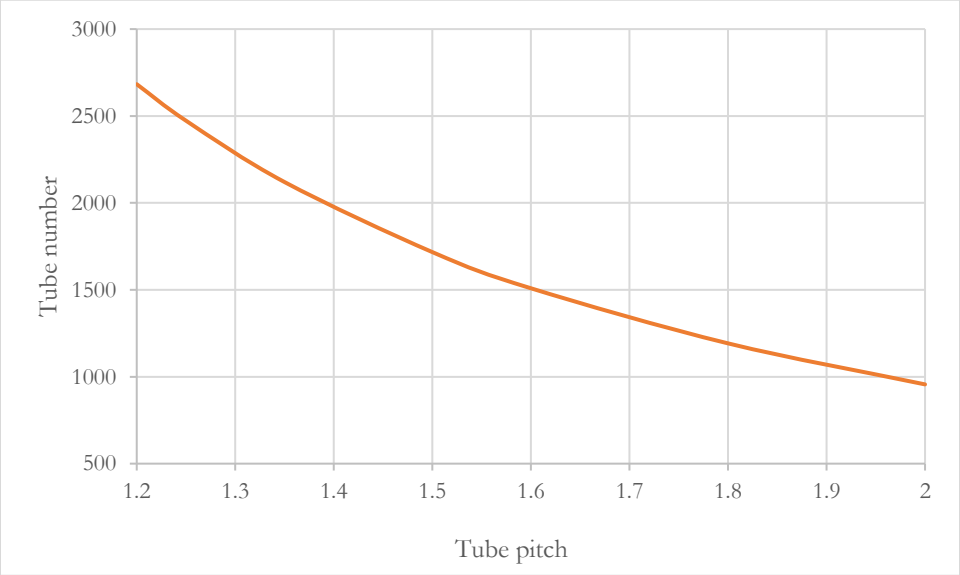

Figure 4. 15: Effect of Tube pitch on Tube number

4.13 Selected shell and tube heat exchanger

The selected shell and tube heat exchanger parameters are shown in Table 4.16. The selection was made while considering a reasonable pressure drop for both the shell and tube side, the desirability to have a significant ratio for shell diameter to tube length, and a design consideration that allows for a reduced number of tubes and material cost represented by the volume of tube materials.

Table 4. 16: Design parameters for the selected heat exchanger

Design parameters for shell and tube heat exchanger device	
Number of Passes	1
Shell inner diameter(m)	8.00
Shell outer diameter(m)	8.15
Tube inner diameter(m)	0.102
Tube outer diameter (m)	0.110
Number of Baffles	8
Tube Pitch	$1.6 \times d_o$
Number of Tubes	1509
Baffle spacing (m)	5.6
Length of tube (m)	51.62
Shell side pressure drop (bar)	2.17
Tube side pressure drop (Pa)	360.92
Overall heat transfer coefficient (W/m^2K)	60.51
Overall surface area for heat transfer (m^2)	24852

5.0 CFD CALCULATION USING ANSYS-FLUENT

5.1: Ansys-Fluent simulation

The ANSYS fluent software was used in simulation of the shell and tube heat exchanger device. The design details below are the values used in building the prototype of the selected heat exchanger device. The prototype is a 1/10000 th reduction of the original model due to the limitation of the computation resource. The simulation provides the qualitative support to design of the heat exchanger.

5.2 Temperature distribution of device

Figures 5.1 to 5.5 show the temperature distribution of the air and CO_2 fluid flowing through the heat exchanger device. This was done using the ANSYS 18.1 software. The geometry was built in the design modeler and meshing was developed with over a million nodes and three million elements. Boundary and cell zone conditions were added in the set-up for the inlet and outlet. The shell has inlet temperature of 1500 K, and mass flow rate of 760.01 kg/s. The tubes have inlet temperature of 450 K and mass flow rate of 806.74 kg/s. Inconel 617 was selected as the shell and tube material with properties listed in Table 3.1, shell fluid was air and tube fluid was CO_2.

The temperature distribution of the air fluid is presented in Figure 5.1. High temperature air at about 1500 K flows into the top part of the shell and move to the bottom part of the shell where the temperature falls to about 1300 K and later falls to about 800 K due to heat transfer from air to the CO_2 through the Inconel 617 tubes. As shown in Figure 5.2, CO_2 fluid at 450 K enters into the Inconel 617 tubes and gain heat from hot air thereby increasing to about 800 K at halfway through the tube length and reaching 1000 k towards exit of the tubes. As shown in Figure 5.3, the wall of the shell material is at elevated temperature of about 1220 K to 1350 K at around the body of the shell and falls to between 800 K – 900 K towards the shell outlet. As shown in Figure 5.4, the Inconel 617 tubes shows elevated temperature of 940 K – 1080 K at most part of the tube length, which is between the

temperature of air and CO_2. Figure 5.5 shows a sectional view of the shell and tube heat exchanger with air and CO_2 fluid running through the shell and tubes, respectively.

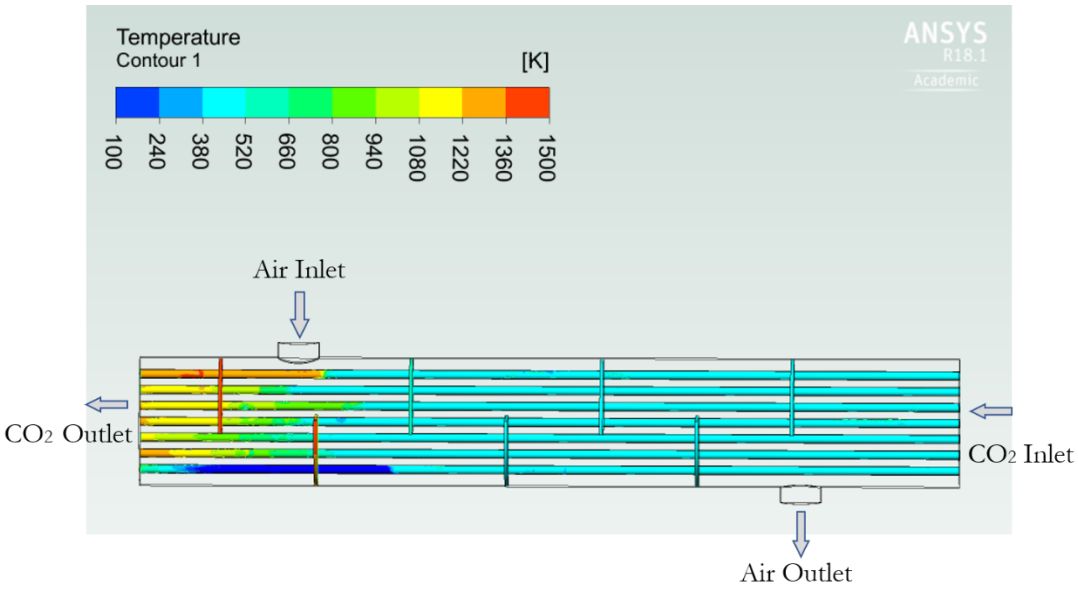

Figure 5.1: Temperature distribution of CO_2

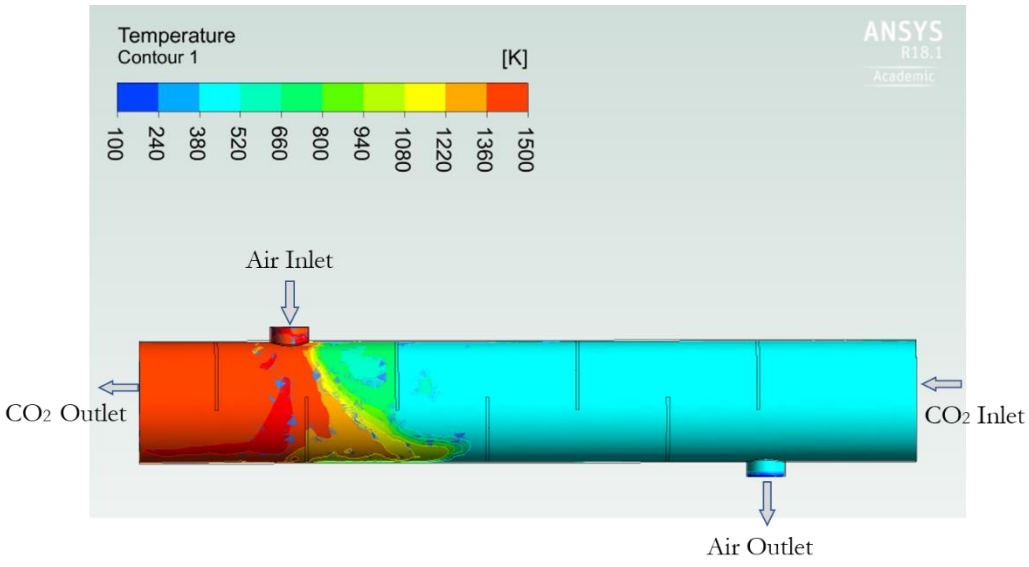

Figure 5.2: Temperature distribution of air

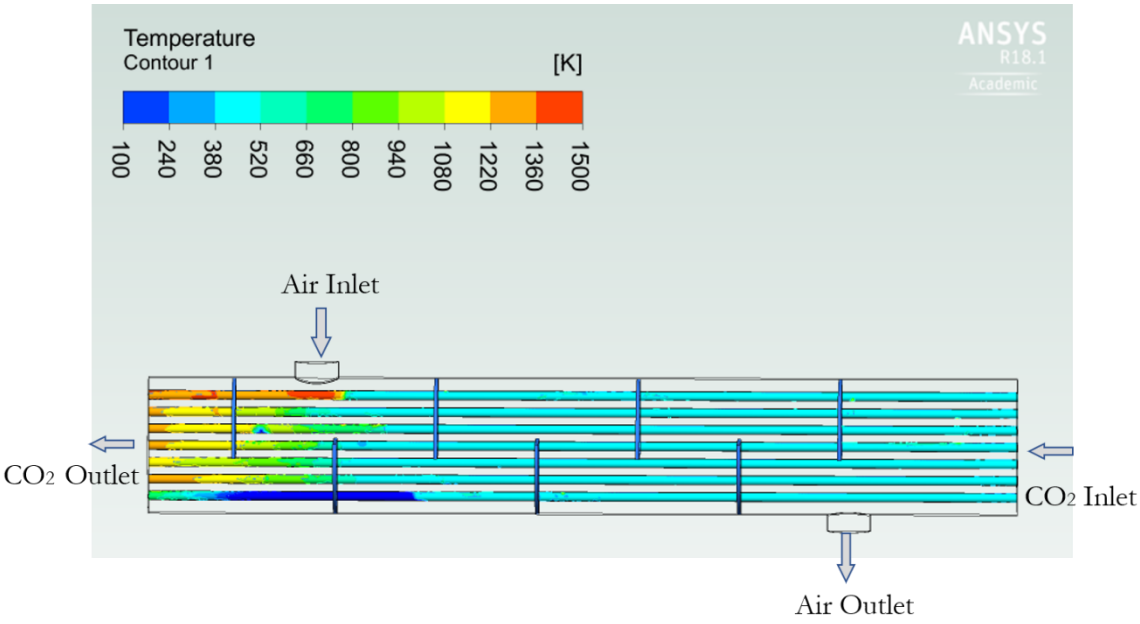

Figure 5.3: Temperature distribution of tubes

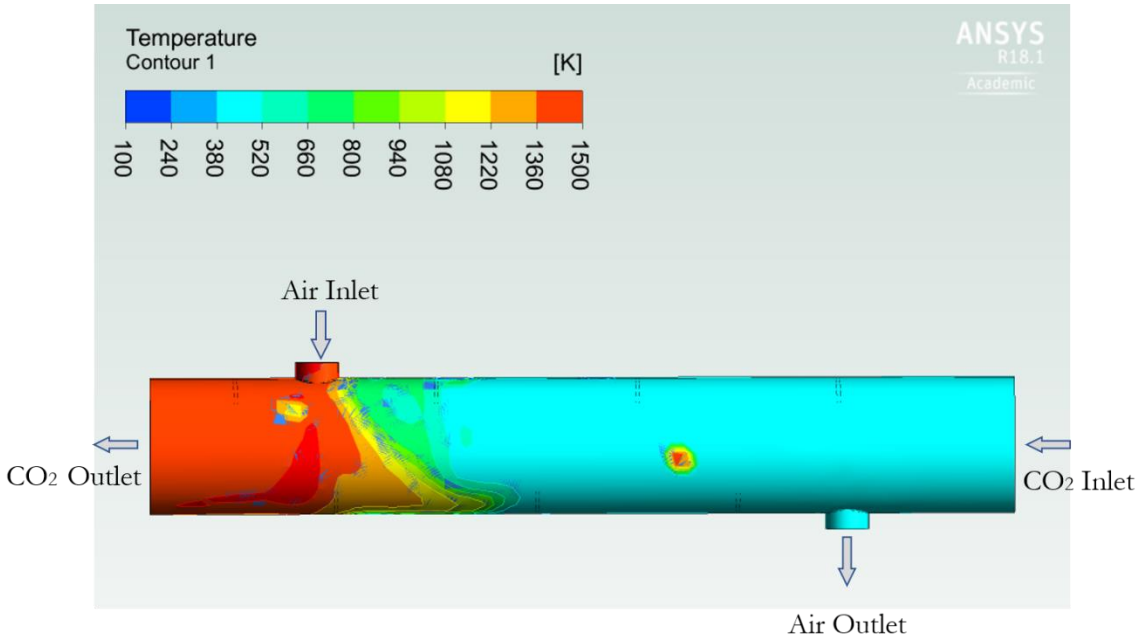

Figure 5.4: Temperature distribution of shell

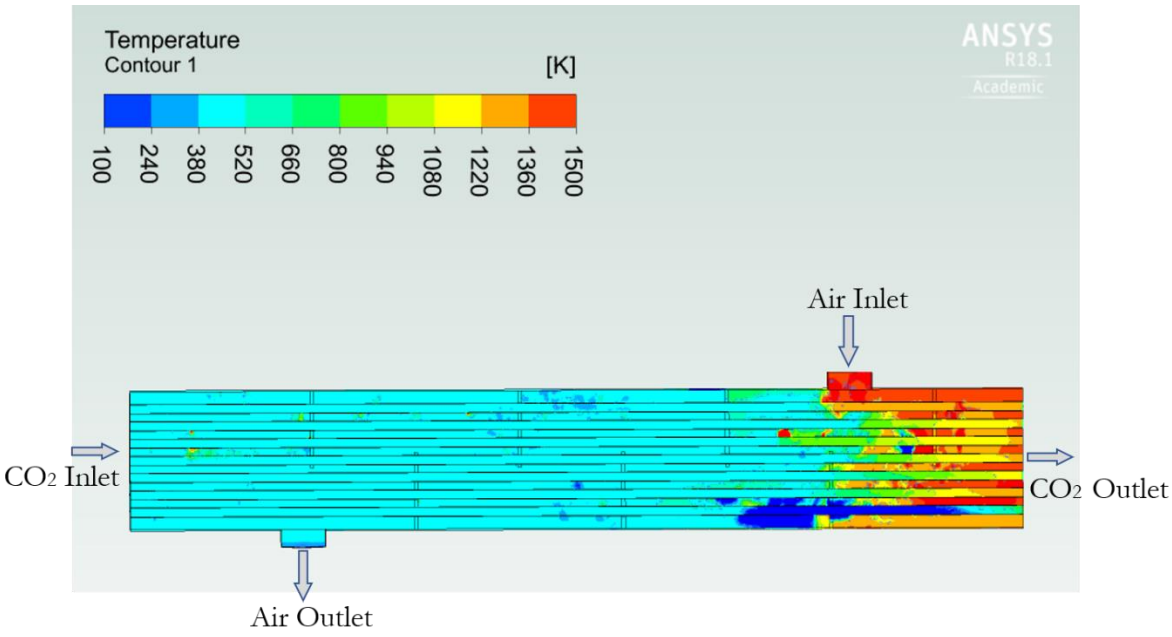

Figure 5.5: Temperature distribution in central line of heat exchanger device

5.3 Thermal analysis

The thermal analysis was done using ANSYS 18.1 software. The engineering data for Inconel 617 was added as presented in Table 3.1 while the geometry was built, and edge and body size meshing were done. The loading conditions were added as temperatures conditions on shell inlet, shell outlet, shell side region, tube inlet, tube outlet and tube side region. The temperature distribution was calculated and evaluated and presented in Figure 5.6 while Figure 5.7 plots the variation of the allowable stress with changes in temperature along the tubes. The result below shows how the shell and tube material conduct heat when hot air flows into it. Maximum temperature of 1500 K is observed at air inlet region and minimum temperature of 450 K to 600 K is observed at CO_2 inlet. An average temperature of 1047.8 K to 1049.3 K is seen around the inside surface of the tube. The variation in temperature of the Inconel 617 material under loading further buttress its quality of high thermal.

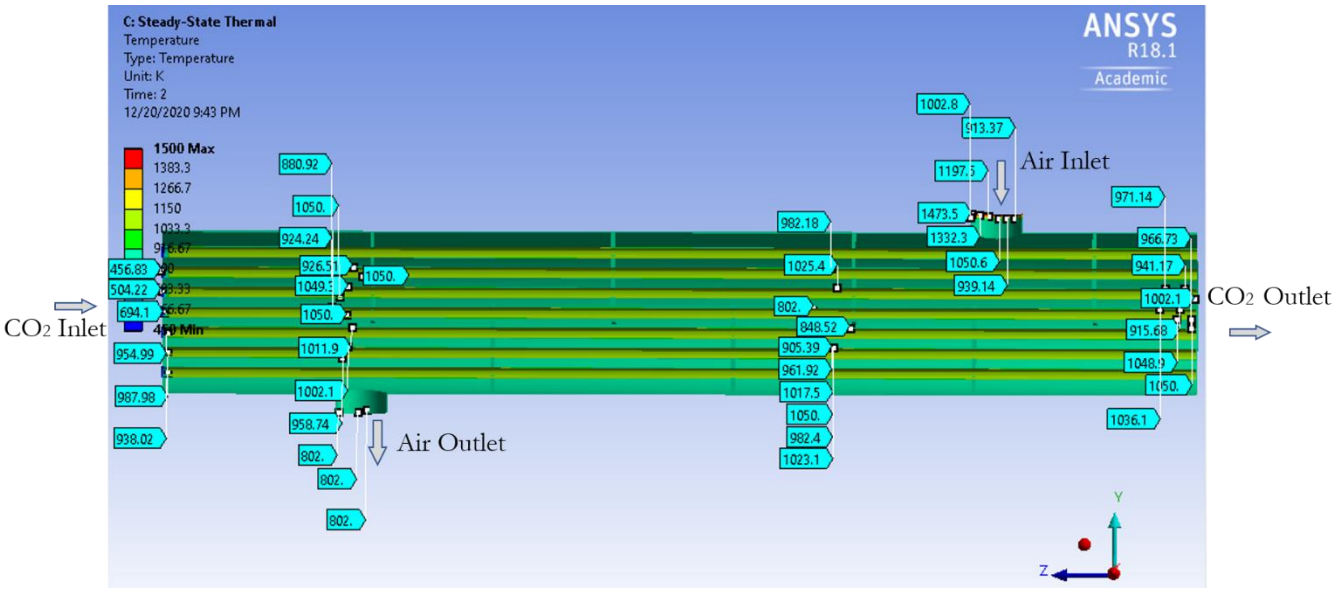

Figure 5.6: Thermal analysis of heat exchanger device

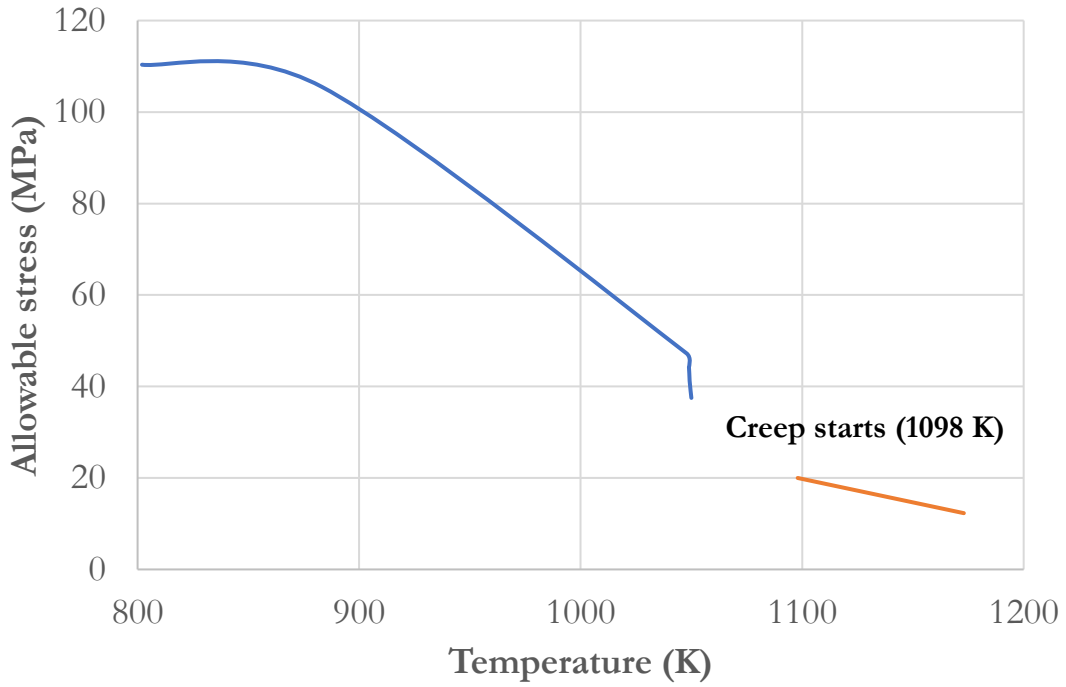

Figure 5.7:Variable of the allowable stress with changes in temperature

6.0 CONCLUSION AND FUTURE WORK

6.1 Conclusion

The procedure designing supercritical CO_2 heat exchanger was developed and applied to design a S-CO_2 heat exchanger for a 300 MW S-CO_2 turbine. The design of a shell and tube heat exchanger was conducted using preliminary equations with several sample tests done using shell diameters values of 6 m to 18 m and tube diameters 0.028 m to 0.12 m. Smaller shell diameter of between 8 m to 12 m is preferable as they offer a limited number of tubes and less volume of shell material , a shell side pressure drop of 0.4 bar to 2.26 bars , tube side pressure drop of 20.63 Pa to 110.05 Pa, increased overall heat transfer coefficient of 33.26 W/m^2K to 57.31 W /m^2K.

It could also be concluded that smaller tubes values of 0.083 m to 0.12 m are good for construction as they offer higher overall heat transfer coefficient of 52.51 W/m^2K to 59.35 W/m^2K and shell side pressure drop of 2.23 bar to 2.35 bar.

The main geometry parameters of the shell and tube heat exchanger designed include shell diameter 8 m, tube diameter 0.102 m, and pitch of 1.6$\times$ d_o. The calculated length of shell is 51.62 m. There are 1509 tubes used with a total length of 77894.58 m. The overall heat transfer coefficient calculated is 60.51 W/m2k. The pressure drop of air in shell calculated is 2.17 bar while the pressure drop of CO_2 in the tubes was 360.92 Pa.

The CFD simulation provides detailed distribution of temperature of fluids, shell and tubes, and material strength.

6.1 Future works

This design work is only done for a square-pitch layout and can be extended for a triangular pitch layout for heat transfer analysis on shell and tube heat exchanger for selected applications. Also, the

design work was restricted to a one-pass tube system and can be tested for a two-pass and three-pass exchanger system.

A CFD simulation of full-scale heat exchanger should be conducted once the computational resource is made available. It is expected that the CFD simulation will help to verify if the system designed can achieve the heat transfer needed.

REFERENCES

[1] "What Are Supercritical CO_2 Power Cycles?" https://www.powermag.com/what-are-supercritical-co2-power-cycles/ (accessed Dec. 18, 2020).

[2] T. J. Held, "Supercritical CO_2 cycles for gas turbine combined cycle power plants."

[3] Y. Ahn et al., "Review of supercritical CO_2 power cycle technology and current status of research and development," Nuclear Engineering and Technology, vol. 47, no. 6. Korean Nuclear Society, pp. 647–661, Oct. 01, 2015, doi: 10.1016/j.net.2015.06.009.

[4] A. Meshram et al., "Modeling and analysis of a printed circuit heat exchanger for supercritical CO_2 power cycle applications," Appl. Therm. Eng., vol. 109, pp. 861–870, Oct. 2016, doi: 10.1016/j.applthermaleng.2016.05.033.

[5] P. Friedman and M. Anderson, "Thermodynamics," in Fundamentals and Applications of Supercritical Carbon Dioxide (SCO_2) Based Power Cycles, Elsevier Inc., 2017, pp. 41–66.

[6] E. M. Clementoni and T. L. Cox, "Effect of compressor inlet pressure on cycle performance for a supercritical carbon dioxide brayton cycle," in Proceedings of the ASME Turbo Expo, Aug. 2018, vol. 9, doi: 10.1115/GT2018-75182.

[7] S. Sullivan et al., "Grant O. Musgrove Heat Exchangers for Supercritical CO_2 Power Cycle Applications Tutorial: Additional contributions from: Lalit Chordia Marc Portnoff."

[8] "Organic Rankine cycle - Wikipedia." https://en.wikipedia.org/wiki/Organic_Rankine_cycle (accessed Dec. 18, 2020).

[9] S. Quoilin, M. Van Den Broek, S. Declaye, P. Dewallef, and V. Lemort, "Techno-economic survey of organic rankine cycle (ORC) systems," Renewable and Sustainable Energy Reviews, vol. 22. Pergamon, pp. 168–186, Jun. 01, 2013, doi: 10.1016/j.rser.2013.01.028.

[10] H. Seo, J. E. Cha, J. Kim, I. Sah, and Y.-W. Kim, "Design and Performance Analysis of a Supercritical Carbon Dioxide Heat Exchanger," Appl. Sci., vol. 10, no. 13, p. 4545, Jun. 2020, doi: 10.3390/app10134545.

[11] D. Shiferaw, J. M. Carrero, and R. Le Pierres, "Economic analysis of S-CO_2 cycles with PCHE Recuperator design optimisation."

[12] "Department of Energy Announces $128 Million for Sustainable Transportation Research | Department of Energy." https://www.energy.gov/articles/department-energy-announces-128-million-sustainable-transportation-research (accessed Dec. 18, 2020).

[13] M. Huang, C. J. Tang, and A. Mcclung, "Steady State and Transient Modeling for the 10 MWe SCO_2 Test Facility Program," 2018.

[14] S. Kung, J. Shingledecker, I. Wright, A. Sabau, B. Tossey, and T. Lolla, "The 6 th International Supercritical CO_2 Power Cycles Symposium Corrosion of Heat Exchanger Alloys in Open-Fired S-CO_2 Power Cycles."

[15] Q. Zhu, "Innovative power generation systems using supercritical CO_2 cycles," Clean Energy, vol. 1, no. 1. Oxford University Press, pp. 68–79, 2017, doi: 10.1093/ce/zkx003.

[16] "Heat exchanger - Wikipedia." https://en.wikipedia.org/wiki/Heat_exchanger (accessed Dec. 18, 2020).

[17] R. Brogan, "Shell and tube heat exchangers," in A-to-Z Guide to Thermodynamics, Heat and Mass Transfer, and Fluids Engineering, Begellhouse.

[18] D. Ameta, "Shell and Tube Heat Exchanger," Int. J. Progress. Sci. Technol., vol. 5, no. 2, pp. 49–52, 2017, Accessed: Dec. 18, 2020. [Online]. Available: http://ijpsat.ijsht-journals.org.

[19] K. Wusiman and Z. Zhou, "Investigation of Shell and Tube Heat Exchanger with Disc-and-Doughnut Baffles," OALib, vol. 07, no. 09, pp. 1–10, Sep. 2020, doi: 10.4236/oalib.1106762.

[20] S. H. Gawande, S. D. Wankhede, R. N. Yerrawar, V. J. Sonawane, and U. B. Ubarhande, "Design and Development of Shell & Tube Heat Exchanger for Beverage," Mod. Mech. Eng., vol. 02, no. 04, pp. 121–125, 2012, doi: 10.4236/mme.2012.24015.

[21] "Shell & tube heat exchanger equations and calculations - EnggCyclopedia." https://www.enggcyclopedia.com/2019/05/shell-tube-heat-exchanger-equations/ (accessed Dec. 18, 2020).

[22] "Dry Air Properties." https://www.engineeringtoolbox.com/dry-air-properties-d_973.html (accessed Dec. 18, 2020).

[23] "Forging Capabilities and Guide Video | Ferrous And Non Ferrous Metals." https://super-metals.com/industrial-resources/page/2/ (accessed Dec. 18, 2020).

[24] I. G. Wright, B. A. Pint, J. P. Shingledecker, and D. Thimsen, "Materials considerations for supercritical CO_2 turbine cycles," in Proceedings of the ASME Turbo Expo, Nov. 2013, vol. 8, doi: 10.1115/GT2013-94941.

[25] "Inconel 617 Tech Data." http://www.hightempmetals.com/techdata/hitempInconel617data.php (accessed Dec. 18, 2020).

[26] "How to Calculate Mawp." https://sciencing.com/calculate-mawp-8516775.html (accessed Dec. 18, 2020).

[27] "[PDF] Incropera S Principle Of Heat And Mass Transfer Download Online – eBook Sumo PDF." https://ebooksumo.com/search/incropera-s-principle-of-heat-and-mass-transfer/

(accessed Dec. 18, 2020).

[28] "Carbon dioxide - Prandtl Number." https://www.engineeringtoolbox.com/carbon-dioxide-prandtl-number-viscosity-heat-capacity-thermal-conductivity-d_2024.html (accessed Dec. 18, 2020).

[29] R. Dodd, "Thermal design of shell and tube heat exchangers.," no. March, 1983.

[30] Songgang Q.,"hX (1)," Renewable Energy, no. c. west virginia university, Morgantown, West Virginia, pp. 241403–241403, 2008.

APPENDIX 1 . Orthographic projection of heat exchanger device